Oil & Natural Gas Technology

DOE Award No.: DE-NT0006553

Progress Report
Second Half 2010

ConocoPhillips
Gas Hydrate
Production Test

Submitted by:
ConocoPhillips
700 G Street
Anchorage, AK 99501
Principal Investigator: David Schoderbek

Prepared for:
United States Department of Energy
National Energy Technology Laboratory

January 31, 2011

Office of Fossil Energy

Disclaimer

Executive Summary

Accomplishments

- Working interest co-owner approval for proposed production test site was received.
- Well and Test Designs were advanced and reviewed with NETL. Given the complexity of the test, it will be completed in two seasons with drilling and logging accomplished in 2011 and production testing following in 2012.

Current Status

- Work is underway to secure permits to drill and log the well in Q1, 2011.
- Work continues to refine the design for 2012 activities including well completion, injection, production processes, and data gathering.
- Efforts to simulate reservoir performance continue.

Introduction

Work began on the ConocoPhillips Gas Hydrates Production Test (DE-NT0006553) on October 1, 2008. This report is the seventh progress report for the project and summarizes project activities from July 1, 2010 to December 31, 2010. A major milestone was achieved October 29th when ConocoPhillips received formal co-owner approval to conduct the test in the Prudhoe Bay Unit.

Detailed work on the well design resulted in the well being reconfigured for low-rate CO_2 injection due to recognition that CO2 injection temperature control is not possible at high injection rates. This reconfigured design was reviewed with NETL on December 1st. To accommodate the reconfiguration and minimize technical uncertainty, the test will now be undertaken over 2 seasons. The well will be drilled and completed in 2011, with perforation, injection, flow back, and depressurization conducted in 2012.

Task 3 (Phase 1): Field Site Ownership Negotiations

Task completed: Formal permission to conduct hydrate production test in Prudhoe Bay Unit was received from PBU working interest owners October 29.

Task 4 (Phase 1): Evaluation of Synergies w/Ongoing DOE-BP Arctic North Slope Gas Hydrates Project

Task completed: BP informed ConocoPhillips July 9 that they did not plan to execute field activity for DOE-BP Arctic North Slope Gas Hydrates Project in 2011, nor would they act as operator for ConocoPhillips hydrate production test in Prudhoe Bay Unit.

Task 5 (Phase 2): Detailed Well Planning/Engineering

Significant progress was made in well planning, and a draft well plan was presented to DOE project management team (Ray Boswell and Rick Baker), as well as DOE-selected panel of hydrate experts (Tim Collett, Research Geologist, USGS; Brian Anderson, Assistant Professor, Chemical Engineering, University of West Virginia; Scott Wilson, Senior Vice President, RyderScott; Steve Hancock, Well Engineering Manager, RPS Energy) on December 1. Proposed separation of project into two-winter operation, with drilling, logging, casing, cementing, and completion installation during winter 2011, followed by perforation, injection, flowback/drawdown testing, and P&A in winter 2012 was discussed and affirmed. Plans for 2011, including geological/reservoir evaluation plans, casing design, and completion design are described in detail as follows.

Openhole data collection plans include mudlogging, logging-while-drilling (LWD) of 13½" hole, and full wireline logging suite in 9⅞"hole, including Schlumberger's Platform Express (PEX), Combinable Magnetic Resonance (CMR), Pressure Express (XPT) and Modular Dynamic Tool (MDT) (Figure 1).

Openhole Data Collection Plan
Mudlogging: Surface to Total Depth (2825 ft)
13 1/2" Hole, Mid-Eocene Mudstone (1475 ft) LWD Sperry/Halliburton: GR-Rt-Φ_D-Φ_N
9 7/8" Hole to Total Depth (2825 ft) LWD Sperry/Halliburton: GR-Rt Wireline Schlumberger: PEX-CMR-XPT Drillpipe-conveyed Schlumberger: Dual-packer MDT

Figure 1: Iġnik Sikumi #1 Openhole Data Collection Plan

Drilling and casing design, including approximate proposed setting depths, is summarized in Figure 2. Surface casing will be set in the 13½" hole, drilled to 1475 feet. Drilling to this depth will land the intermediate TD in a 150ft-thick mudstone just above the Sagavanirktok F" sands. These sands are expected to be ice-saturated. Depths may be adjusted slightly if the structural elevation of the formation tops varies. The subsequent "production hole" will be drilled with a 9⅞" bit and chilled oil-base drilling mud to 2825 feet. After logging, a tapered 7⅝" x 4½" casing string will be run and cemented with low heat-of-hydration cement.

Completion design is summarized graphically in Figure 3. 10¾" casing will be cemented in the 13½" surface hole, and a 7⅝" x 4½" tapered casing will be cemented to surface with low heat-of-hydration cement to minimize hydrate dissociation during cement

hydration and curing. The "upper completion" consists of equipment cemented in the hole with the 7⅝" x 4½" tapered casing string. A fiber-optic Distributed Temperature Sensor (DTS) string is shown in yellow and will be clamped outside the tapered casing and run to TD. Three surface-readout pressure/temperature gauges (shown in red) will also be run on the 4½" casing. Electronic lines for these (shown in black) will be clamped to the outside of the tapered string. A bottom gauge will monitor fluid fill-up during completion operations. Both the upper and central gauge will be run above the anticipated perforation interval in Sagavanirktok Upper C sand. A central gauge is placed between the nipple and the seal-bore receptacle, which reflect the top and bottom of a sand-control screen to be run prior to the final depressurization step. (This depressurization step is described in more detail below.) The central gauge will allow pressure and temperature monitoring behind the sand-control screen.

Once the 7⅝" x 4½" tapered casing is cemented, the upper completion is installed on 4½" tubing. This tubing string, when stung into a polish-bore receptacle seal assembly (at the 7⅝" x 4½" crossover) converts the wellbore to a 4½" monobore which simplifies perforation, injection, and flowback testing. Clamped to the outside of the tubing, bound together in a triple flatpack, are three ¾" tubing strings. Two ¾" strings (shown in red) are run open-ended to facilitate fluid circulation and heating of the annulus. This "heater string" allows the 7⅝" x 4½" annulus to act as a heat exchanger, facilitating the delivery of injected fluids at the desired temperature. The chemical injection mandrel (shown in red) has a variable back-pressure valve, which is critical to the delivery of liquid CO_2 to the perforations at sub-breakdown pressure. The chemical injection mandrel is connected to the third ¾" tubing string (shown in blue). This line facilitates the delivery of liquid CO_2 at low to moderate rates. The gas-lift mandrel (shown in blue) serves four functions: evacuation of fluid from the annulus, artificial lift of fluid in the 4½" tubing, installation of an additional pressure-temperature gauge, and as a circulation port for cementing during plug and abandonment (P&A) operations.

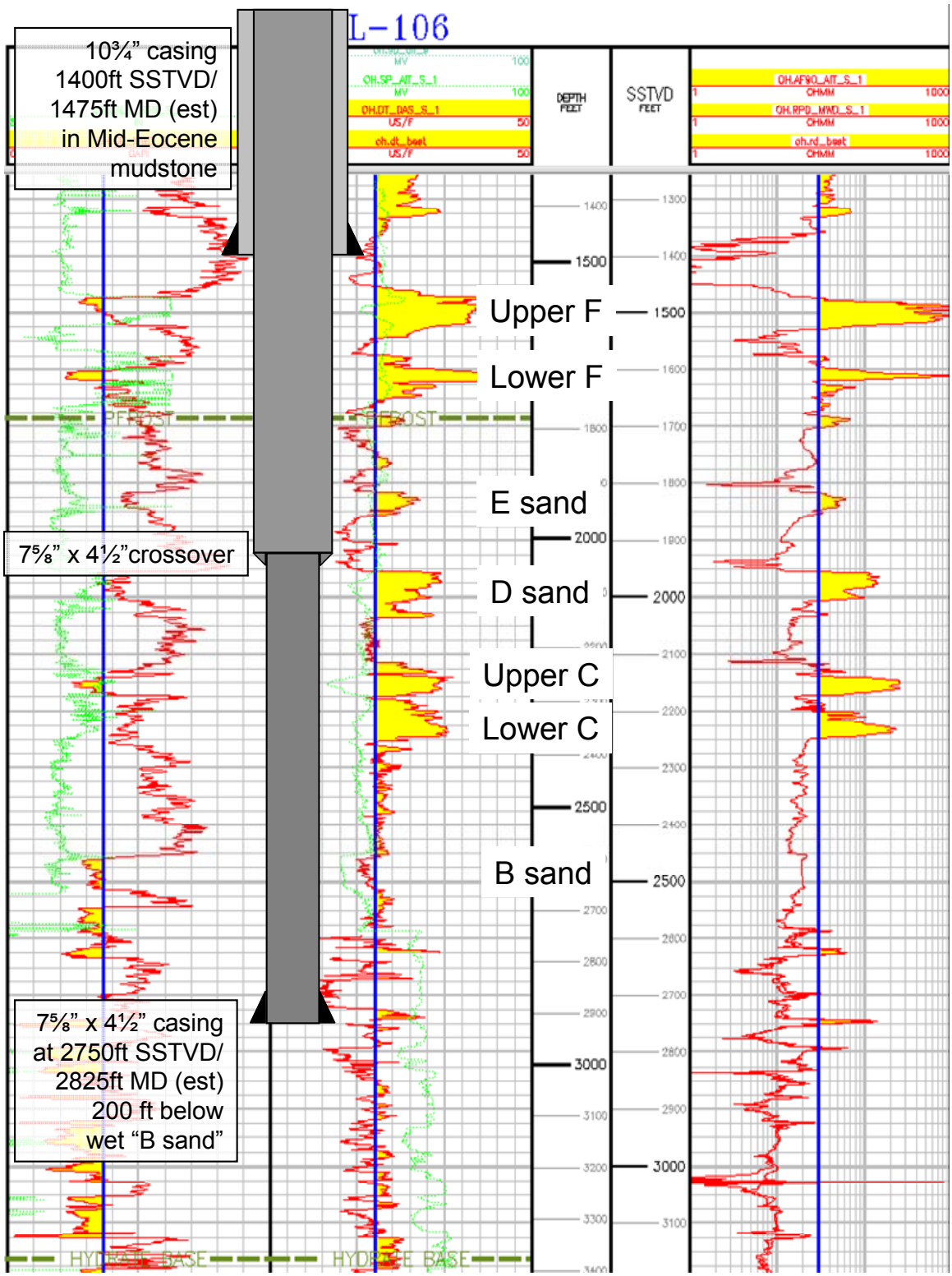

Figure 2: Subsurface stratigraphy and casing plan

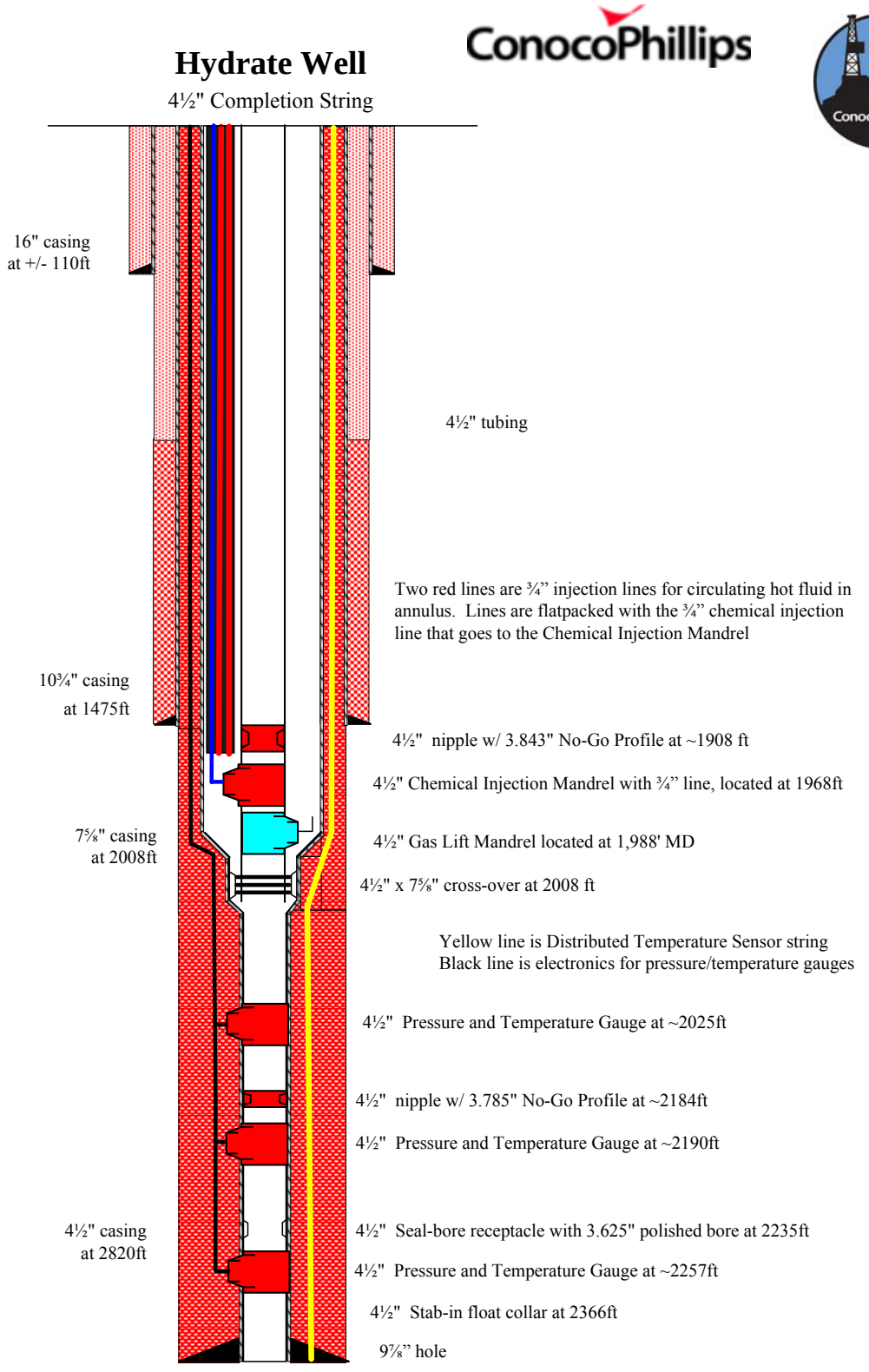

Figure 3: Completion design

Task 6 (Phase 2): Pre-Drill Estimation of Reservoir Behavior

Evaluation of Nitrogen Pre-Flush

An important consideration with CO_2 injection in North Slope hydrate-bearing reservoirs is the impact on permeability when CO2 hydrate forms upon contact with excess free water in the pores. An experiment was designed to evaluate the effectiveness of a nitrogen gas pre-flush on enhancing or preserving permeability in hydrate-saturated sandstone in the presence of excess free water. Results are discussed below.

The sandstone core started with an initial water saturation of 52% prior to hydrate formation. MRI intensity was used in these experiments as a measure of water saturation, and indirectly used to determine hydrate saturation. MRI intensity was normalized to the initial water saturation in the sample (Figure 4). The initial water saturation was not as uniform as preferred for this test with more water found on the bottom half of the core and less water at the ends (Figure 5). Methane was introduced at 1200 psi and 4.0°C, converting most of the water into hydrate. Once formed, the hydrate was distributed more uniformly throughout the core.

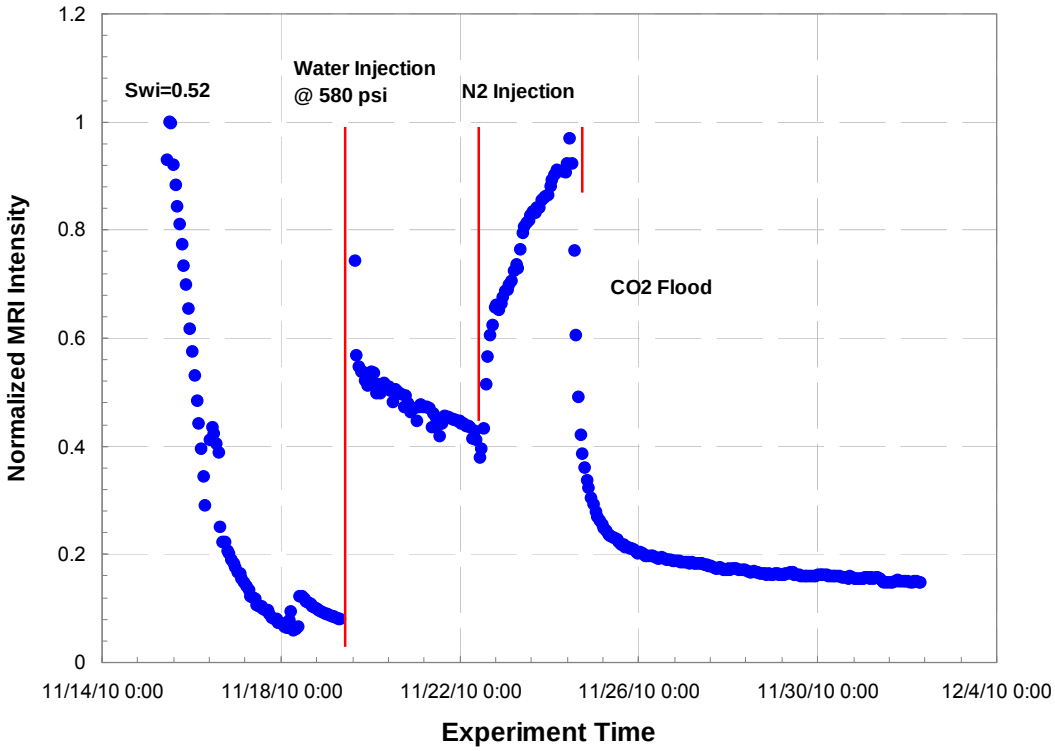

Figure 4. Water saturation as indicated by MRI intensity changed during different stages of the test. The intensity was normalized to initial water saturation of 52%.

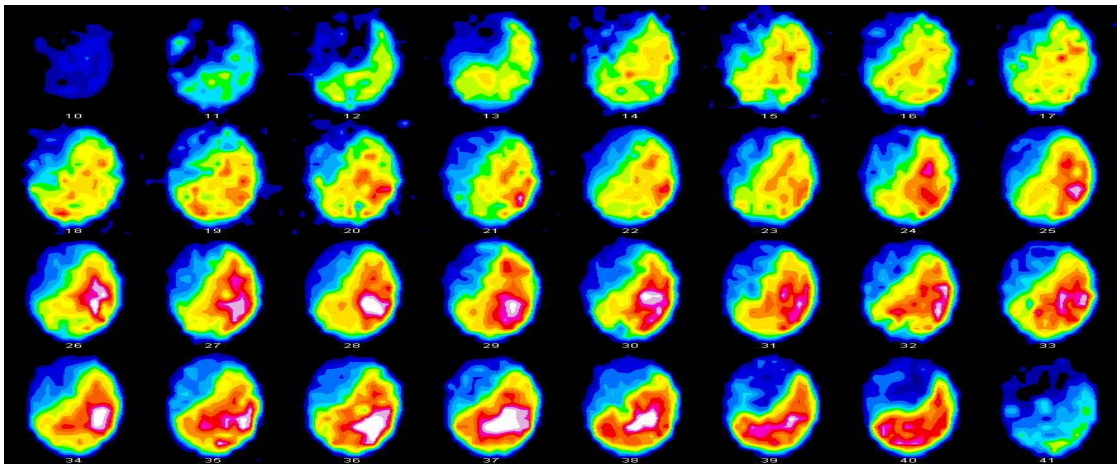

Figure 5. The initial water saturation distribution along the length of the core was somewhat non-uniform as indicated in a series of transverse slices obtained before hydrate formation.

Additional water was then injected into the core in order to create an excess-water system. The formation of methane hydrate was inhibited by reducing the pore pressure to 580 psi. Sufficient water was injected to replace most of the remaining gas-filled free space in the pores with the low-salinity water. The MRI intensity increased to almost the same value as the initial saturation as water filled the remaining pore space (Figure 4). The distribution of the remaining water in the system was more uniform compared to the original saturation (Figure 6). The system was then shut in for several days with methane gas that resulted in the formation of some additional hydrate, raising the total hydrate saturation to approximately 70-80% as illustrated in the MRI intensity decrease (Figure 4).

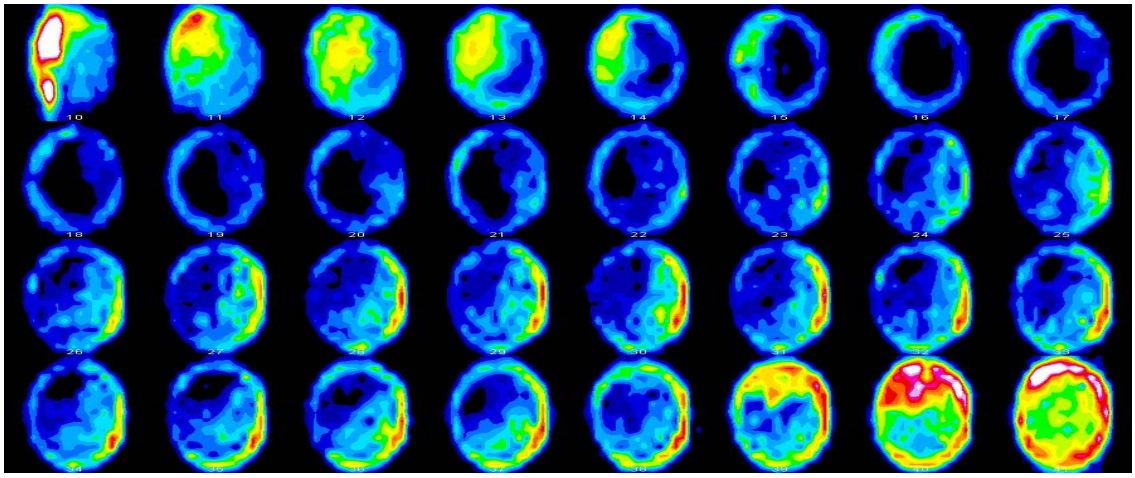

Figure 6. A more uniform distribution of free water in the hydrate-bearing core was obtained after the injection of additional water into the system.

Nitrogen gas was injected at several rates into the hydrate-saturated core. The MRI intensity increase indicated that some of the hydrate was dissociated by the introduction

of nitrogen, creating enough free water comparable to the initial water saturation of 52%. Nitrogen injection caused some hydrate dissociation at the inlet and along the outer edges of the core as evident in a series of MRI images as the N2 pushed some of the water out of the pores (Figure 7).

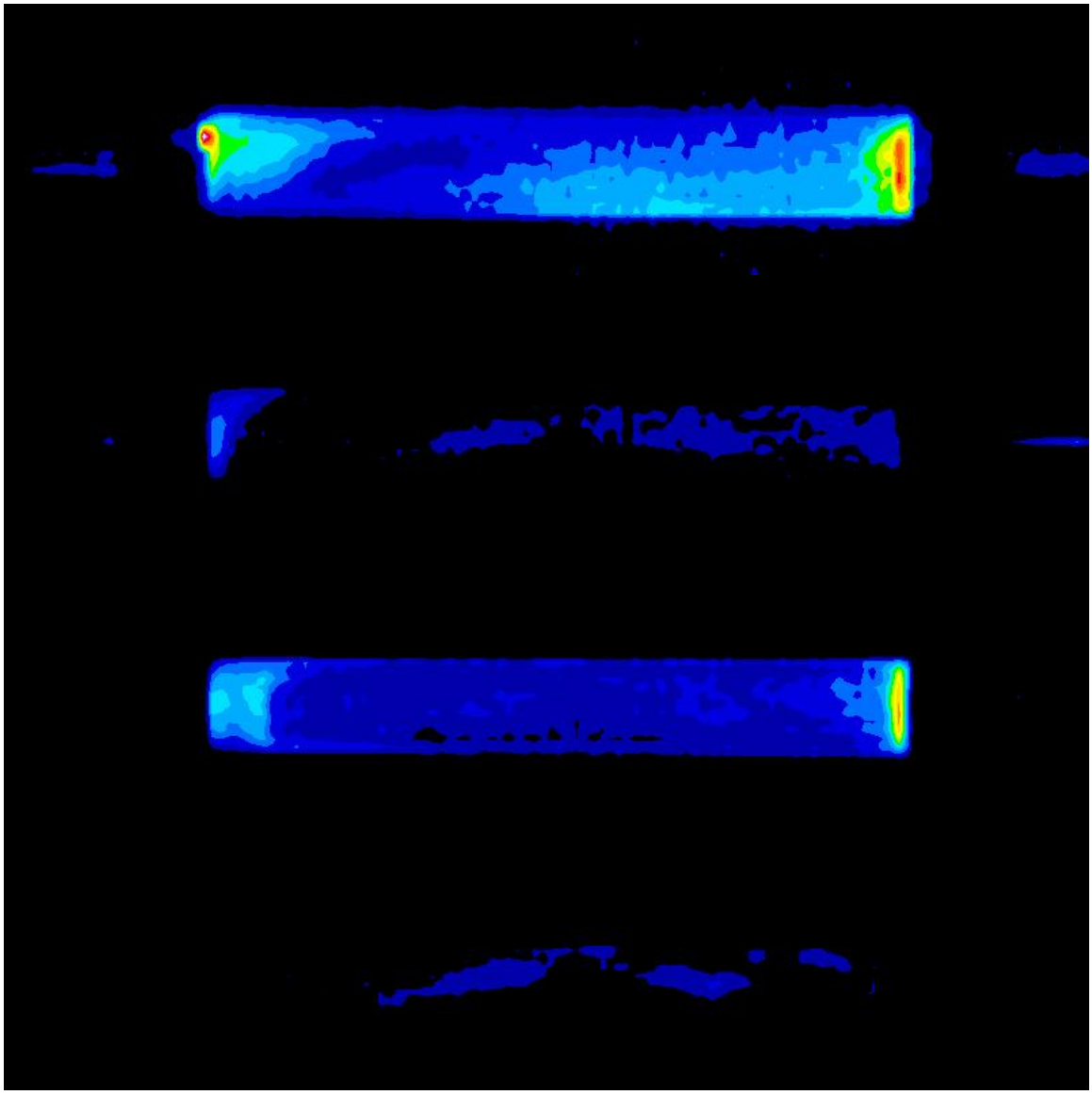

Figure 7. Montage of MRI longitudinal images of average signal intensity indicates water saturation at several stages of test. Top-most image collected after waterflood shows a fairly uniform distribution of excess water in pores. Next image collected after some of the excess water equilibrated with methane and formed additional hydrate, approaching a total saturation of 70-80%. Third image collected after nitrogen flooding shows an increase in water saturation that resulted from hydrate dissociation. Bottom image after CO_2 flood shows most of excess water converted to hydrate. Images are scaled to same brightness and contrast levels.

Nitrogen was allowed to soak for a short period before CO_2 injection, which completed the test. Pressure communication was lost early in the CO_2 injection stage, but was restored after some time (Figure 8). It is not clear whether the stoppage was due to a plug in the lines or within the core. Once pressure communication was re-established, injected CO2 converted excess water in the pores into hydrate. Not all of the remaining free water in the system was converted into a CO_2-hydrate as indicated by the MRI intensity curve.

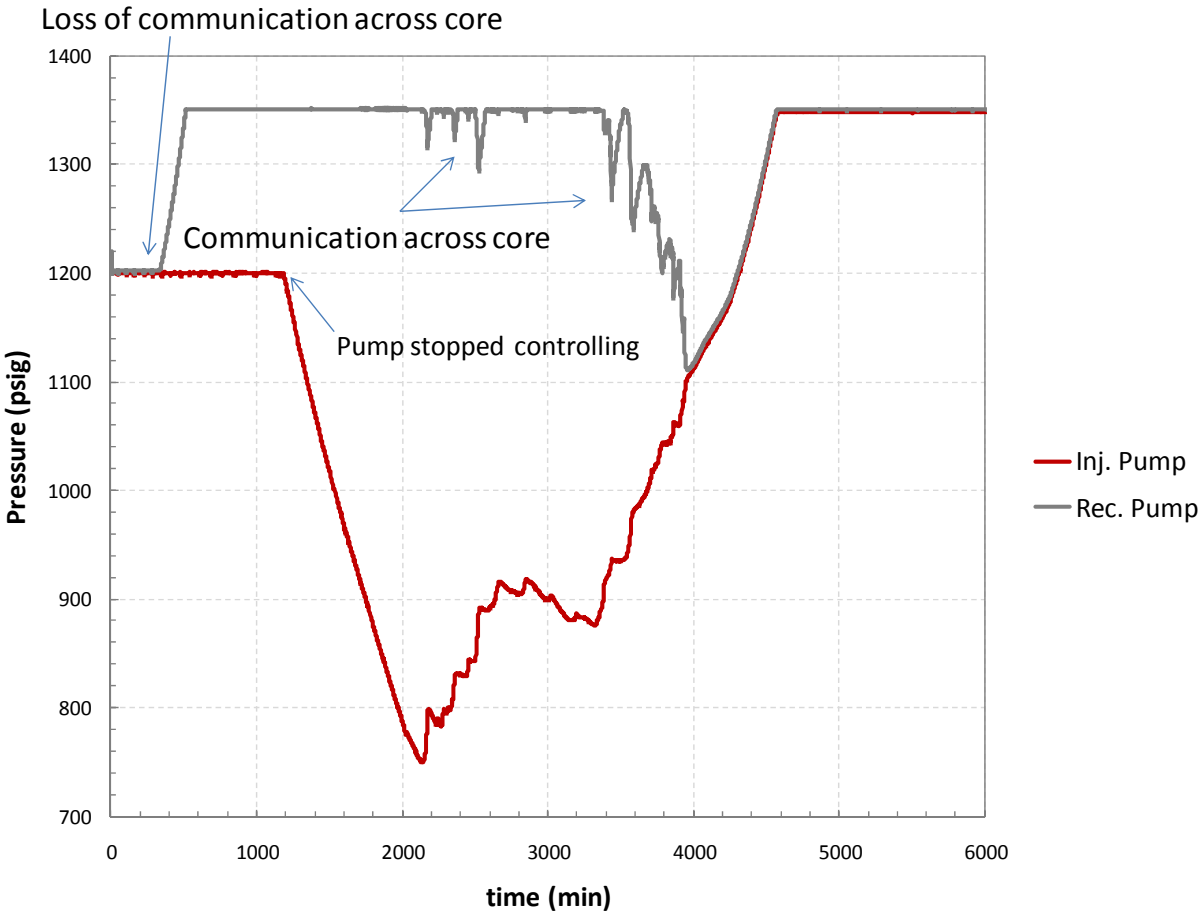

Figure 8. The pump pressures as measured at each end of the core show the loss of communication during the early stages of the CO_2 injection. Over time, communication was re-established across core. It is not know whether the blockage was in the core or the lines.

There were difficulties with this test associated with blockages in the lines due to the presence of excess water, especially after nitrogen injection displaced a considerable volume of moveable water. The MRI images indicated that the nitrogen displacement was not uniform, but rather was concentrated at the edges of the core holder. This is of concern and needs to be evaluated further in light of injection rates and displacement mechanisms for gas replacing water in porous media. While quantitative results

associated with pressure drops used to monitor permeability changes are affected by the blockages, the MRI images do provide some insights into the mechanisms of nitrogen injection and its effectiveness in displacing excess water prior to CO_2 injection.

Understanding how excess water interacts with the injection of CO2 will be a continued focus of experiments in 2011. The experimental challenge of line blockages is being addressed by several modifications to the test design. Improved differential pressure measurements and greater confidence in the gas-liquid mass balance are necessary to understand how any pre-treatment can reduce the impact of additional hydrate formation associated with CO2 injection.

Modeling Depressurization

In May, 2010, a proposal was advanced to combine the ConocoPhillips gas hydrate production test (this project) with a long-term depressurization test from L-Pad in the Prudhoe Bay Unit. Two directional wellbores were proposed with lateral isolation between bottom-hole locations to minimize interference between the tests. Reservoir simulation was performed to determine the radius affected by a two-year depressurization in the Sagavanirktok "Upper C" sandstone (Appendix 1). Depressurization results were then integrated into a full 3D geomechanical simulator to predict changes in reservoir strength and to model compaction and subsidence as depressurization proceeds (Appendix 2).

Appendix 1: A two-year depressurization with 400psi bottomhole pressure was simulated using the 3D geocellular model described in "ConocoPhillips Gas Hydrate Production Test, Progress Report First Half 2010." Two saturation models were used to populate the model: hydrate saturation heterogeneity from the Archie equation and the "AIM model." Details of these two models can be found in "ConocoPhillips Gas Hydrate Production Test Progress Report Second Quarter 2009." The AIM hydrate saturation model predicts rates that increase to 173 bbl water/day and 37 mcf gas/day at the end of 2 years. Cumulative water and gas production at the end of 2 years are 109,000 bbl and 18 mmcf, respectively. The Archie hydrate saturation model predicts rates that increase to 106 bbl water/day and 14 mcf gas/day at the end of 2 years. Cumulative water and gas production at the end of 2 years are 59,000 bbl and 6.3 mmcf, respectively.

Appendix 2: Two-year depressurization results provided input for geomechanical modeling to simulate reservoir compaction and surface subsidence as a function of pressure depletion. A full-field 3D geomechanical model, adherent to conservation principles, the effective stress law, and finite element method, was developed. Predicted peak surface subsidence increases with time as gas production by depressurization proceeds. Peak surface subsidence predictions range from 0.006 to 0.118 ft (0.2 to 3.6 cm) after two years of depressurization and production. The AIM model predicts higher subsidence values than the Archie model for all cases studied.

Cost Status

Expenses incurred during this period were below the Baseline Cost Plan as shown in Exhibit 1.

COST PLAN/STATUS									
Project Phase ==>	**Phase 1, Site Ident.**		**Phase 2, Field Test Planning**						
Baseline Reporting Quarter ==>	**Q408**	**Q109**	**Q209**	**Q309**	**Q409**	**Q110**	**Q210**	**Q310**	**Q410**
BASELINE COST PLAN									
Federal Share	0	0	60000	1450000	0	0	0	0	0
Non-Federal Share	325100	499172	390875	333875	170699	0	0	0	0
Total Planned	325100	499172	450875	1783875	170699	0	0	0	0
Cumulative Baseline Cost	325100	824272	1275147	3059022	3229721	3229721	3229721	3229721	3229721
ACTUAL INCURRED COSTS									
Federal Share	0	0	0	0	0	0	0	0	0
Non-Federal Share	121012	182019	262292	341017	237634	340593	232364	224197	422992
Total Incurred Cost	121012	182019	262292	341017	237634	340593	232364	224197	422992
Cumulative Incurred Cost	121012	303031	565323	906340	1143974	1484567	1716931	1941128	2364120
VARIANCE									
Federal Share	0	0	-60000	-1450000	0	0	0	0	0
Non-Federal Share	-204088	-317153	-128583	7142	66935	340593	232364	224197	422992
Total Variance	-204088	-317153	-188583	-1442858	66935	340593	232364	224197	422992
Cumulative Variance	-204088	-521241	-709824	-2152682	-2085747	-1745154	-1512790	-1288593	-865601

Exhibit 1: Cost Plan/Status

Milestone Status

The Milestone Status is shown in Exhibit 2 below.

MILESTONE STATUS REPORT						
#	Task/Subtask Description	Planned Start Date	Planned End Date	Actual Start Date	Actual End Date	Comments
	Field trial site selected	1-Oct-08	31-Mar-09	1-Oct-08	3-Apr-09	Complete
	Partner negotiations completed	15-Feb-09	31-Mar-09	17-Mar-09	29-Oct-10	Complete
	Synergies with DOE-BP project identified	1-Mar-09	31-Mar-09	30-Mar-09	9-Jul-10	Complete
	Well test designed and planned	1-Apr-09	30-Sep-09	10-Mar-09		Ongoing
	Well and reservoir performance predicted	1-Jul-09	31-Dec-09	22-Jun-09		Ongoing
	Field testing completed	1-Jan-10	31-Dec-10			
	Injection and production monitoring completed	1-Apr-10	30-Apr-10			
	Well abandonment complete	1-May-10	31-Dec-10			

Exhibit 2: Milestone Status

Appendix 1: Depressurization Simulation of an Arctic Gas Hydrate Reservoir
Author: Suntichai Silpngarmlert, ConocoPhillips (Houston)

Subsidence is one of the major concerns related to production from gas hydrate reservoirs because formation strength could dramatically decrease when hydrate in pore space is removed. The main objective of this numerical simulation study is to determine field scale subsidence caused by hydrate dissociation during 2 years of depressurization. In this study, a full 3-D (x, y, z) heterogeneous model was constructed to represent a gas hydrate reservoir in the Prudhoe Bay Unit, Alaska North Slope. One-way coupling between TOUGH+Hydrate simulator (flow simulation) and Dynaflow simulator (geomechanical simulation) was implemented in this simulation study.

1. *Model Descriptions and Reservoir Properties for flow simulation study*

A full 3D model with anisotropic and heterogeneous property distribution has been constructed. The model consists of 6 rock layers: D sandstone, D siltstone, Upper C sandstone, Lower C sandstone, C siltstone, and B sandstone. The model drainage area is 7500ft x 7500 ft. There are faults in the eastern and western parts of the reservoir (Figure 1-1). A vertical production well is simulated at the center of the reservoir and is completed only in the Upper C sandstone layer. The k_v/k_h ratio of the entire model was 0.1 ($k_{vertical}$ = 0.1 x $k_{horizontal}$).

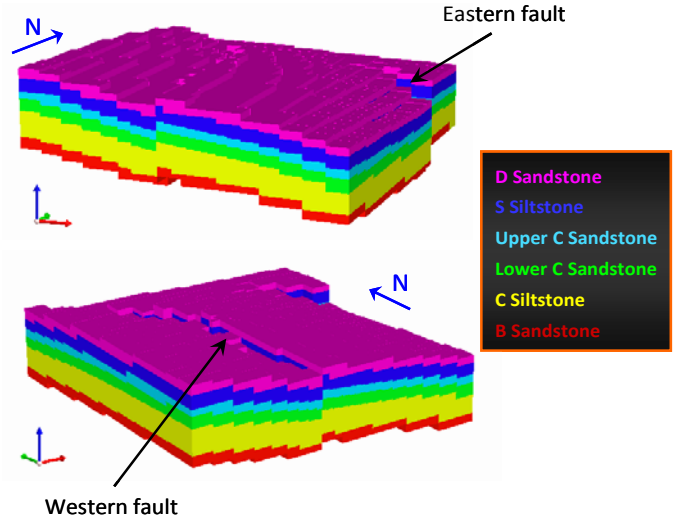

Figure 1-1: Structure of gas hydrate reservoir model used in this study

Figure 1-2 shows areal grid structure of the model used in this study. The model has very small grid blocks around the well to capture flow behavior and hydrate dissociation around the well accurately, since the near-wellbore region is predicted to experience substantial pressure and temperature changes during production. The total number of grid blocks in the model is 287,296 (67x67x64) and lateral grid size ranges from 0.5 to 500 ft and grid thickness is approximately 3.3 ft in the Upper C and Lower C sandstone layers.

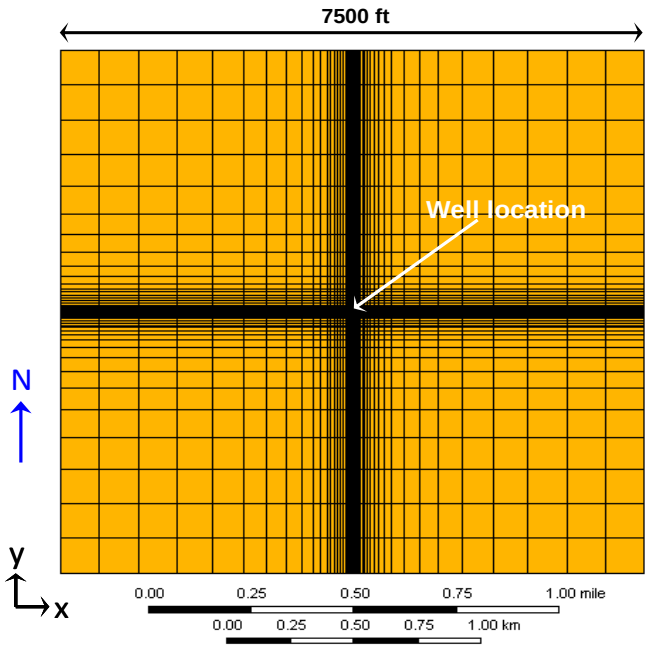

Figure 1-2: Areal grid structure of the model

Table 1.1 summarizes average pore compressibility and irreducible water saturation (Sw_{irr}) in each rock layer

Table 1-1: Pore compressibility and Sw_{irr} for each layer

Layer	Pore compressibility (1/psi)	Sw_{irr}
D sandstone	$12x10^{-6}$	0.10
D siltstone	$17x10^{-6}$	0.32
Upper C sandstone	$12x10^{-6}$	0.12
Lower C sandstone	$11x10^{-6}$	0.11
C siltstone	$16x10^{-6}$	0.25
B sandstone	$21x10^{-6}$	0.06

Initial pressure and temperature in the middle of the completion zone are approximately 975 psi and 42°F, respectively. The initial conditions in the completion zone are well inside in the hydrate stability zone (Figure 1-3) indicating that hydrate present in the completion zone is very stable. Therefore, hydrate dissociation rate is likely to be small resulting in a low gas production rate.

In this simulation study, two cases are examined. Reservoir structure and rock properties of the two cases were the same. However, initial hydrate saturations in Cases 1 and 2 are estimated from different correlations, i.e., AIM (Case 1) and Archie (Case 2) correlations. Figure 1-4 shows the initial hydrate saturations in Cases 1 and 2. Note that missing grid blocks in the D Sandstone layer (Archie-based model) are the grid blocks with zero percent hydrate saturation, which have been excluded from the figure. Initial hydrate saturation in Case 1 ranges from 0.15 to 1.0 (100%). However, the maximum initial

hydrate saturation is limited to 0.8, based on the belief that hydrate saturation greater than 0.8 does not occur in natural gas hydrate reservoirs, which is consistent with the available field data. Initial hydrate saturation in Case 2 ranges from 0.1 to 0.7. The average initial hydrate saturation in Cases 1 and 2 are 0.55 and 0.46, respectively.

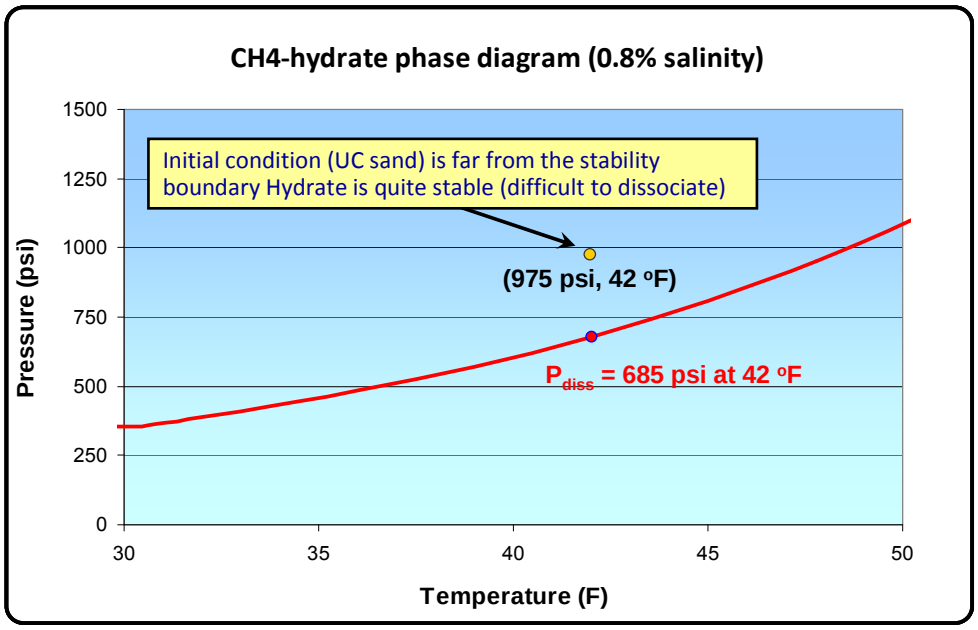

Figure 1-3: Initial condition in the completion zone on CH_4-hydrate phase diagram

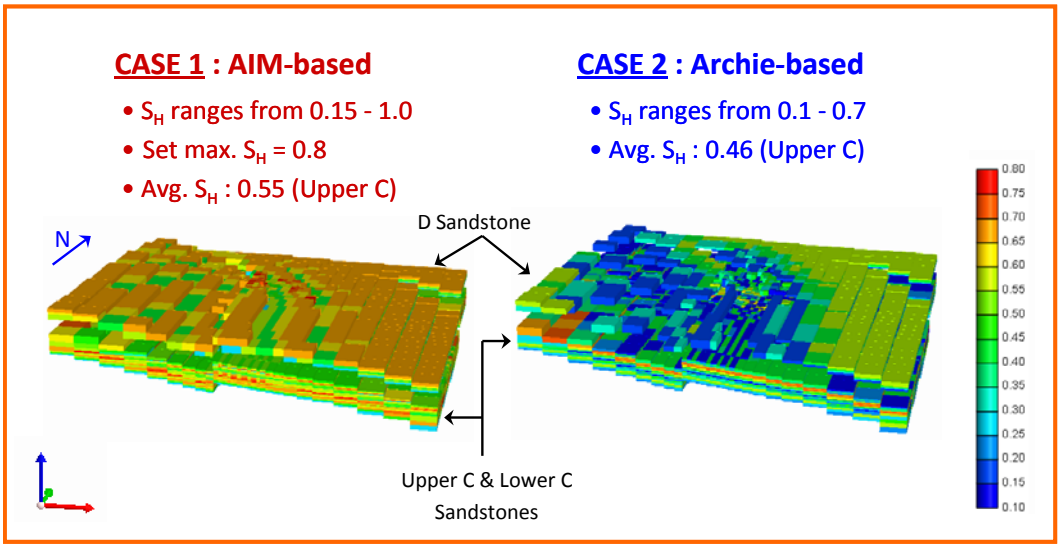

Figure 1-4: Initial hydrate saturation in AIM-based and Archie-based models

1.1 Simulation Results

In this simulation study, the production well is operated with constant bottom-hole pressure (BHP) at 400 psi. Operating at BHP lower than 400 psi may cause ice formation around the well which will block fluid flow toward the well. Note that the pressures at quadruple points (for $CH_4 + H_2O$ + hydrate system) at 0.0% and 0.5% water salinity are about 380 psi and 405 psi, respectively.

1.1.1 Case 1: AIM-based model

Figure 1-5 illustrates that the pressure transient does not intersect the model boundaries at the end of 2 years. This indicates that the modeled drainage area is large enough for this simulation study. Because the dissociation pressure is approximately 680 psi at initial reservoir temperature (42°F), hydrate dissociation only occurs in the blue and dark blue regions, which are very small compared to the size of the reservoir. Figure 1-6 shows non-uniform hydrate dissociation around the well as expected. Note that the pressure map (Figure 1-5) is 7500 ft x 7500 ft, whereas the hydrate saturation map (figure 1-6) is 1700 ft x 1700 ft.

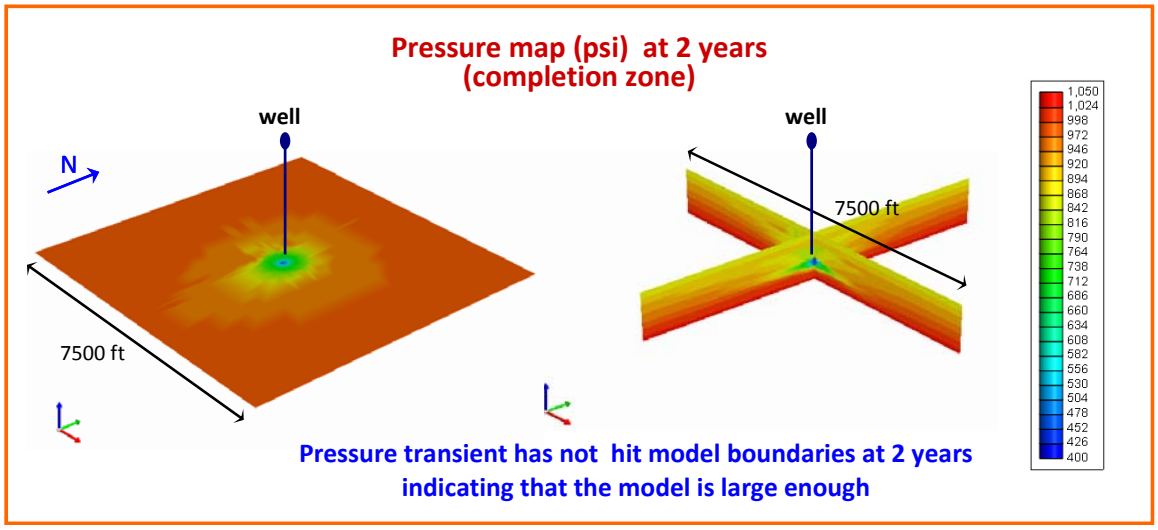

Figure 1-5: Pressure map at the end of 2 years

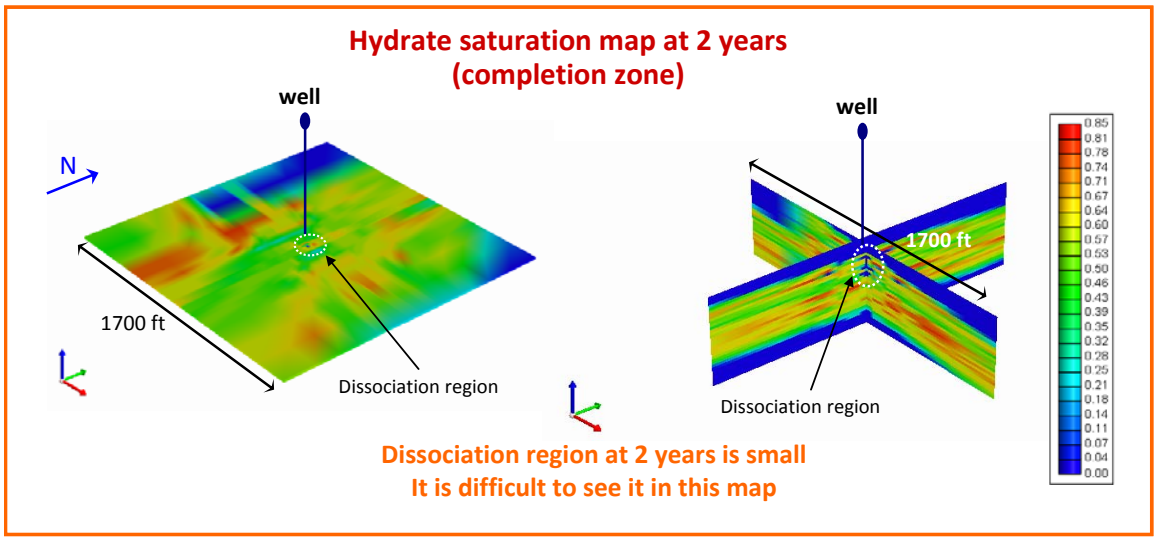

Figure 1-6: Hydrate saturation map at the end of 2 years

It is easier to see the dissociation region, i.e., the low temperature region, in the temperature map (Figure 1-7), since hydrate dissociation consumes energy. A free gas saturation map is the best map to show the hydrate dissociation region in this study. Figure 1-8 indicates that the hydrate dissociation region in this case is about 400 ft in diameter around the well.

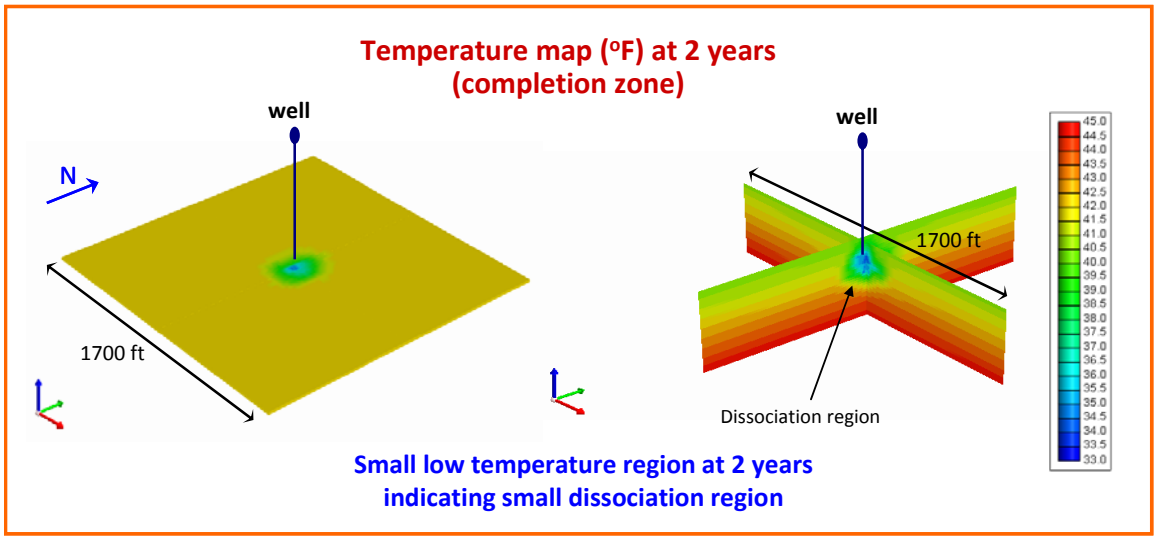

Figure 1-7: Temperature map at the end of 2 years

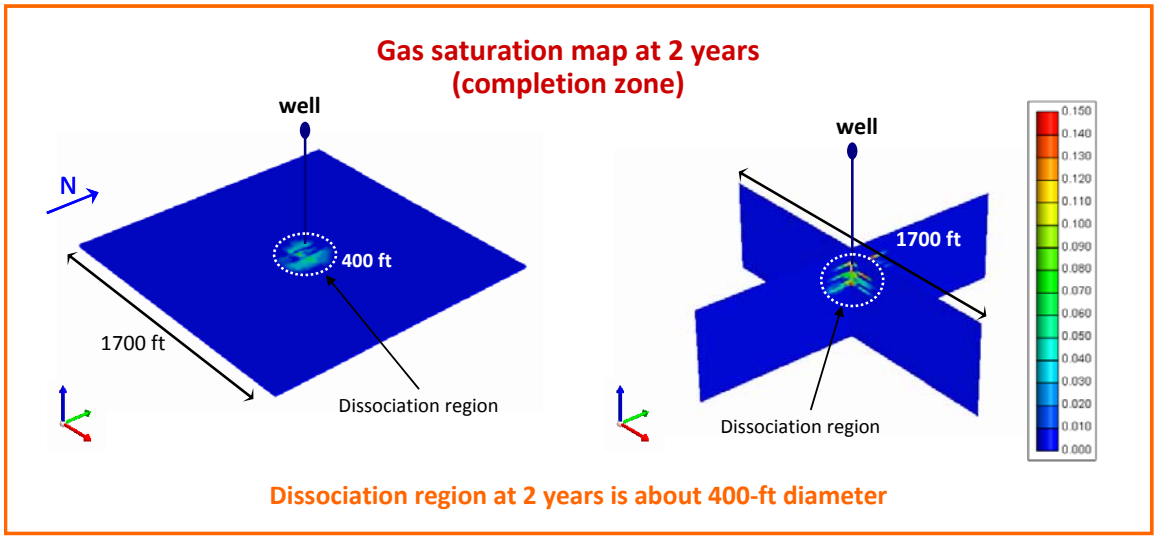

Figure 1-8: Gas saturation map at the end of 2 years

Figure 1-9 shows gas and water production rates predicted during the 2-year depressurization. The water production rate gradually increases to 173 bbl/day, whereas the gas production rate increases to 37 MSCF/day at the end of 2 years. Cumulative gas and water productions at the end of 2 years are 18 MMSCF and 109,000 bbl, respectively.

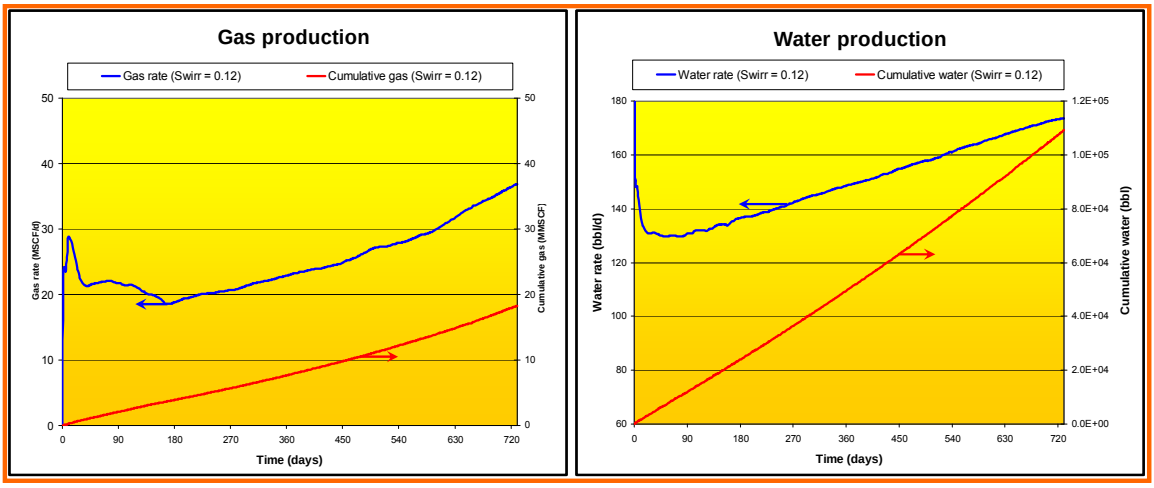

Figure 1-9: Gas and water production rates during 2-year depressurization

1.1.2 Case2: Archie-based model

Figure 1-10 illustrates that the pressure transient does not reach model boundaries at the end of 2 years. This indicates that the model drainage area is large enough for this simulation case.

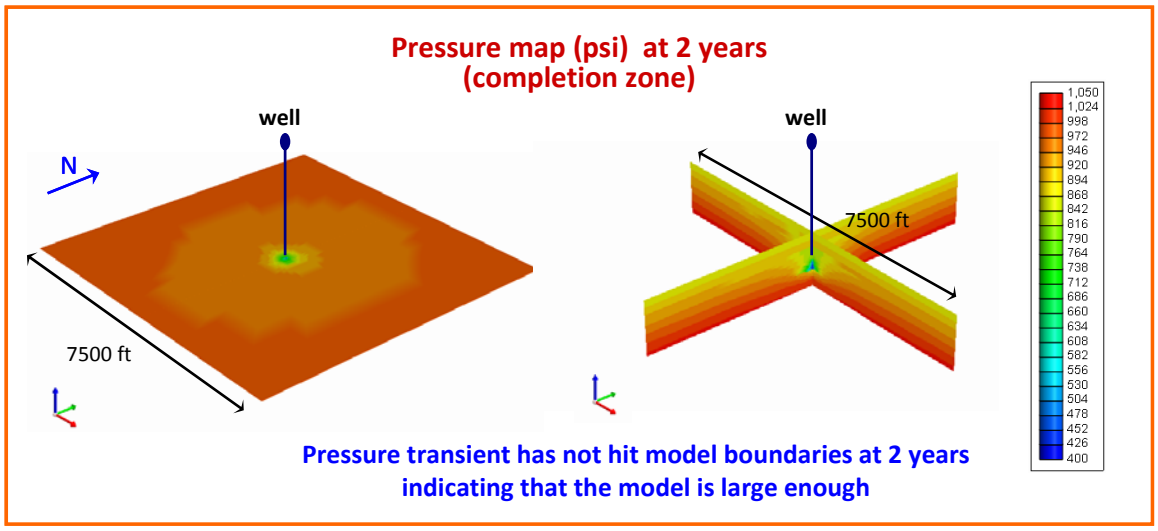

Figure 1-10: Pressure map at the end of 2 years

As mentioned in the previous section, hydrate dissociation is only predicted in the blue and dark blue regions of the map. In this case, they are even smaller than those in Case 1. Case 2 has a lower dissociation rate resulting in lower gas production. Similar to Case 1, Figure 1-11 shows non-uniform hydrate dissociation around the well. Note that the blue regions farther away from the production well initially have zero percent hydrate saturation. There is no hydrate dissociation taking place in these regions.

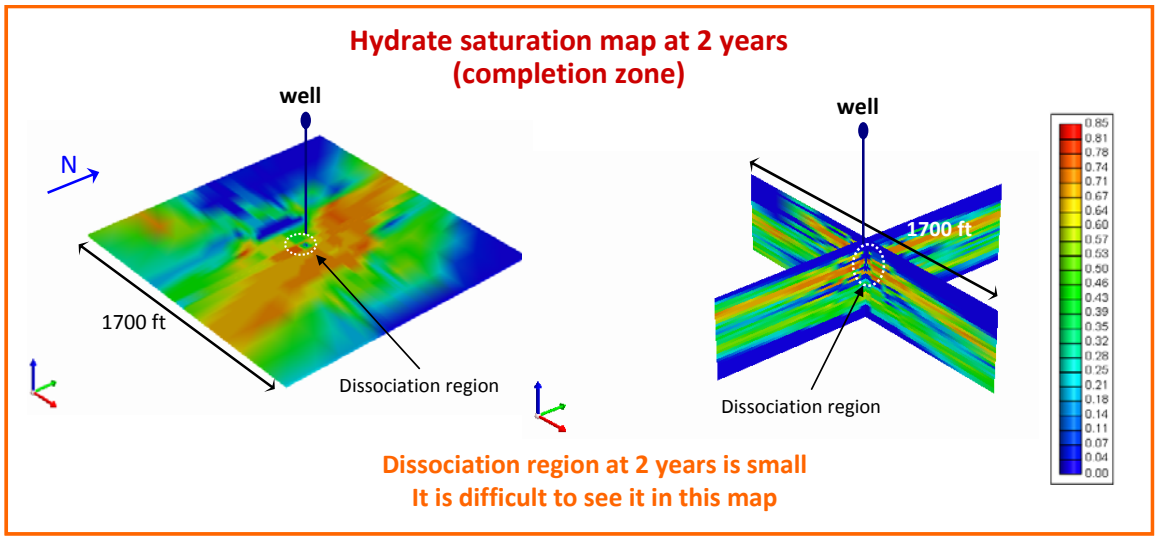

Figure 1-11: Hydrate saturation map at the end of 2 years

Again, it is easier to see the dissociation region (low temperature region) on the temperature map (Figure 1-12).

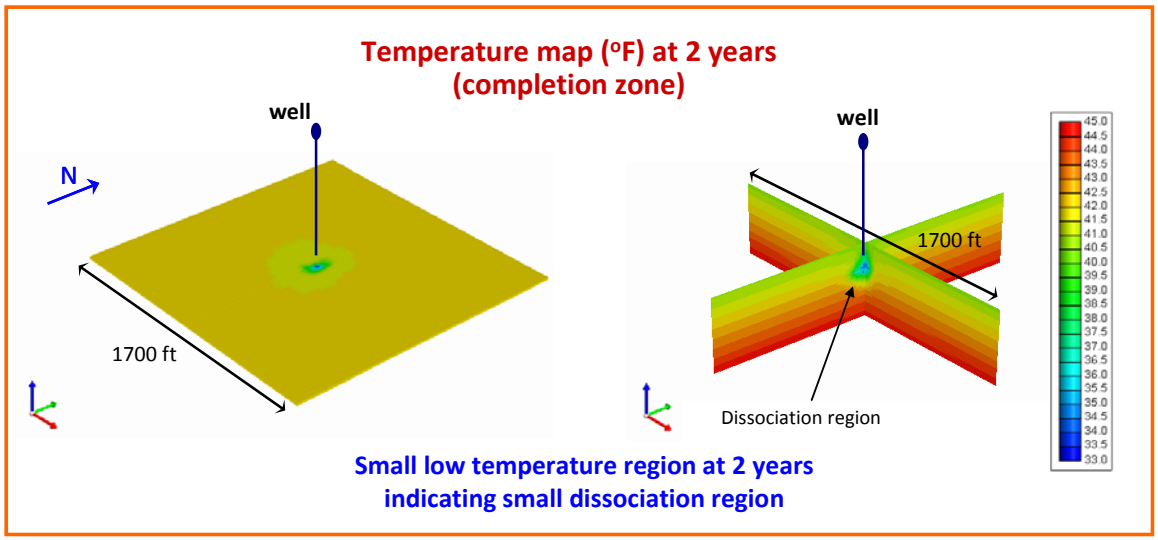

Figure 1-12: Temperature map at the end of 2 years

Figure 1-13 (gas saturation map) indicates that the hydrate dissociation region is about 300 ft in diameter around the production well which is smaller than that in Case 1.

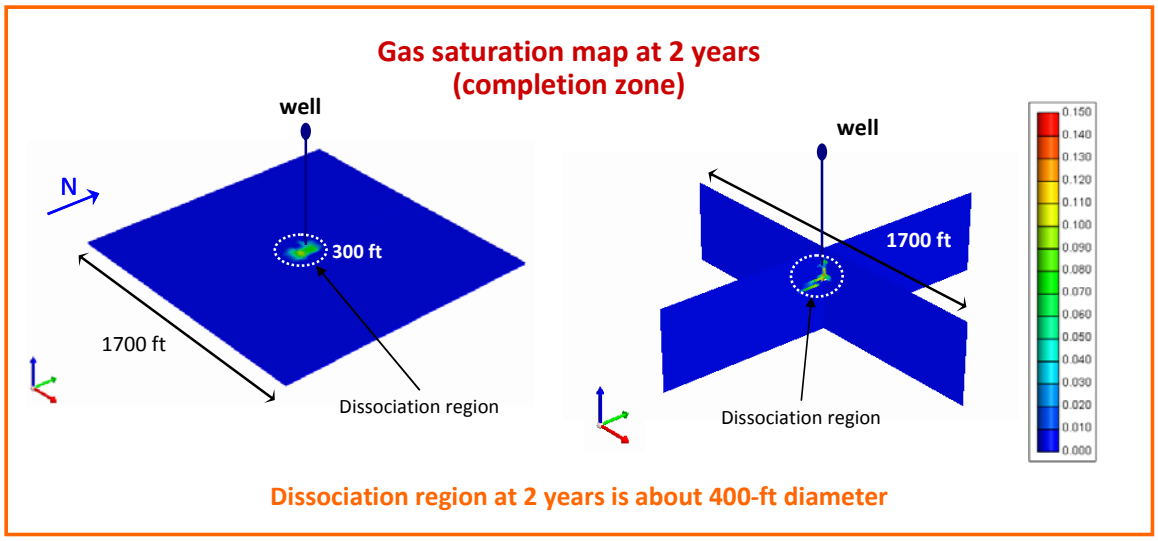

Figure 1-13: Free gas saturation map at the end of 2 years

Figure 1-14 shows gas and water production rates during a 2-year depressurization. The water production rate gradually increases to 106 bbl/day at the end of 2 years, whereas the gas production rate increases to 14 mcf/day, which was lower than that in Case 1 as expected. Cumulative gas and water production at the end of 2 years were 6.3 mmcf and 59,000 bbl, respectively.

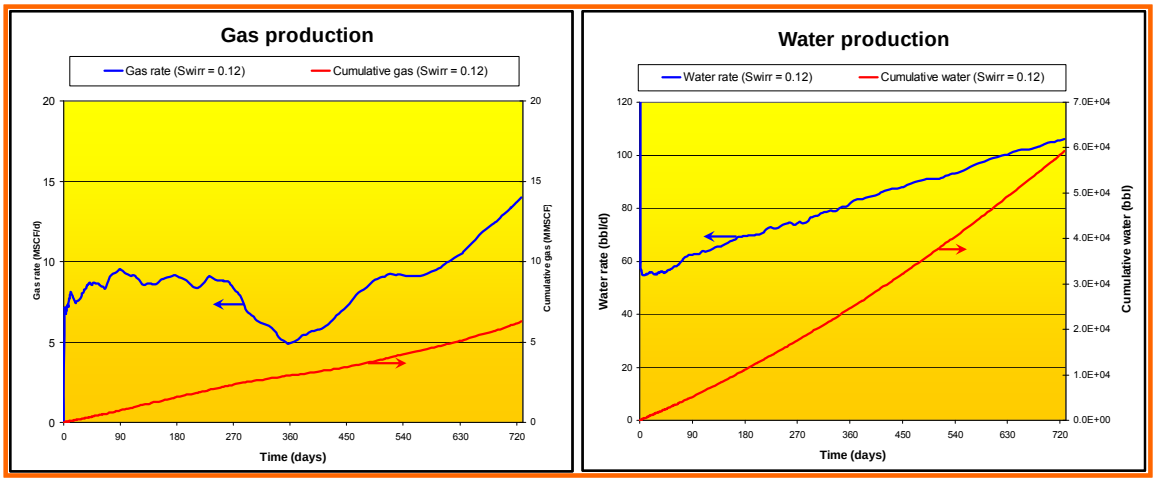

Figure 1-14: Gas and water production rates during 2-year depressurization

AIM-based model vs. Archie-based model

Figure 1-15 compares water and gas production profiles from the AIM-based and Archie-based models. Since initial hydrate saturation near the well in the Archie-based model is higher than that in the AIM-based model, the in-situ permeability around the well region is lower in the Archie-based case. Accordingly, the water production rate in the Archie-based case is lower (106 bbl/d vs 173 bbl/d), resulting in a slower pressure decline and lower hydrate dissociation rate around the well. Consequently, the Archie-based model yields a lower gas production rate (14 mcf/d vs 37 mcf/d at 2 years). Cumulative gas productions at the end of 2 years in Archie-based and AIM-based cases were 6.3 mmcf and 18 mmcf, respectively.

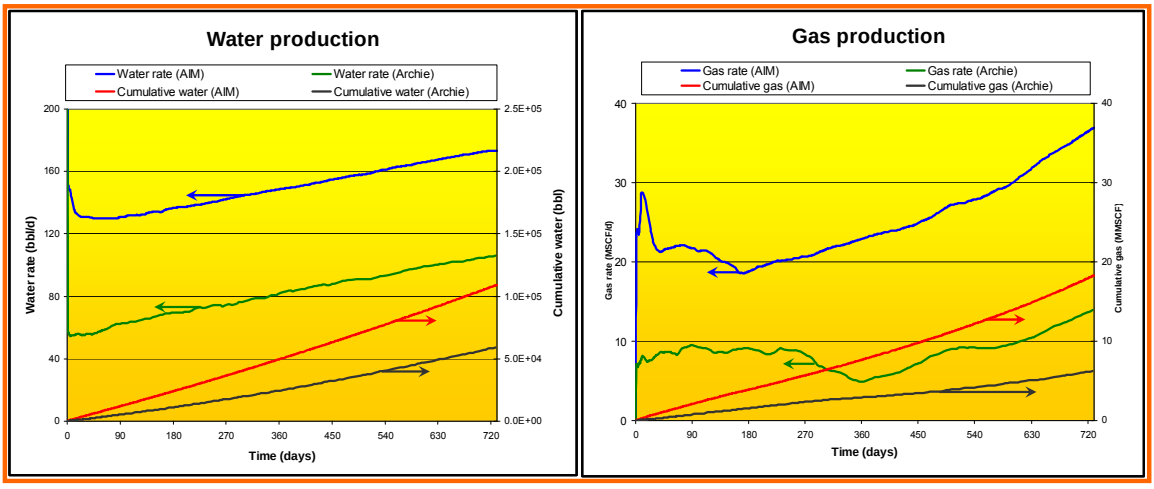

Figure 1-15: Water and gas production profiles in AIM-based and Archie-based models

1.1.3 *Impact of irreducible water saturation (Sw_{irr}) on production behavior*

Figure 1-16 illustrates the predicted production profiles for the AIM-based and Archie-based models with different irreducible water saturations (12% vs. 19%) in the completion zone (Upper C sandstone layer). Note that the 12% cases are the base-cases which were discussed in Sections 1.2.1, 1.2.2, and 1.2.3. Note that setting irreducible water saturation 20% or more will prohibit water flow in the grid blocks that have 80 percent hydrate saturation. Therefore, the irreducible water saturation was set at 19% to allow water flow in every grid block of the model.

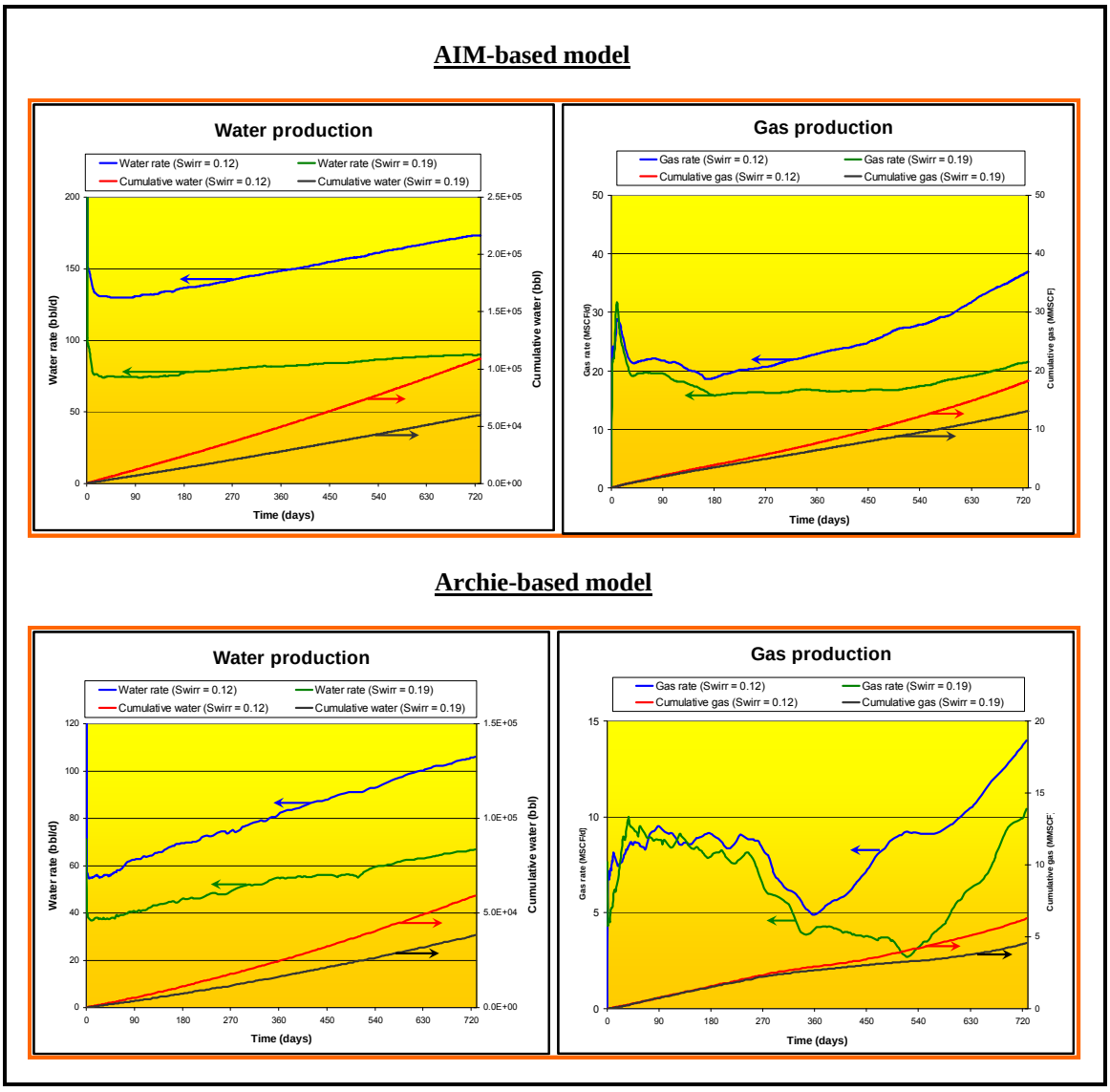

Figure 1-16: Impact of irreducible water saturation on production profiles

As expected, in both AIM-based and Archie-based models, 19% irreducible water saturation cases yield lower water and gas production rates because these cases have lower in-situ permeability resulting in slower pressure decline around the well. The gas

rates at 2 years for the AIM-based and Archie-based cases with 19% Sw_{irr} are 22 mcf/d and 10.4 mcf/d, respectively.

1.2 Conclusions for flow simulation study

- This study modeled a shallow North Slope gas hydrate reservoir with pressure and temperature characteristics of the C Sand. Pressure decline in the modeled this Arctic gas hydrate reservoir is not very high because the initial pressure of the reservoir is not high and bottom hole pressure (BHP) needs to be controlled above the pressure at the quadruple point during production to avoid ice formation around the well which can cause plugging problems.

- Variations in production performance between AIM-based and Archie-based models emphasize the importance of high quality estimates of reservoir properties, especially initial hydrate saturation.

- Production via depressurization (from the modeled Arctic gas hydrate reservoir) from a vertical well yields low rates of gas production. Though not modeled herein, horizontal wellbores or wells producing near the base of the gas hydrate stability zone are expected to deliver gas at higher rates.

The results predicted by these flow simulations (pressures, temperatures, saturations at various times during 2-year depressurization,) provided inputs for geo-mechanical simulation, results of which are discussed in the following section.

Appendix 2: Surface Subsidence Prediction for Gas Production of Methane Hydrate Reservoirs by Pressure Depletion on the North Slope of Alaska
Author: Lee Chin, ConocoPhillips (Houston)

I. Introduction

Changes in reservoir pressure during gas production by pressure depletion from a methane hydrate reservoir can induce reservoir compaction and subsidence at the earth's surface. The purpose of this study is to quantify the impact of gas production by pressure depletion from the methane hydrate reservoir on surface subsidence in the PBU L-pad area. Specifically, the study's objectives are: 1) to build a full-field, three-dimensional geomechanical (Dynaflow) model for predicting subsidence under gas production by pressure depletion from the methane hydrate reservoir at the PBU L-pad area; 2) to use the developed model to conduct surface subsidence predictions based on pressure maps of the gas production cases by pressure depletion obtained from the PBU L-pad TOUGH+Hydrate reservoir model; and 3) to generate contour maps showing predicted surface subsidence and vertical displacement for the cases studied.

This study develops a full-field, 3D geomechanical subsidence model to predict surface subsidence using a numerical method of computing the magnitude of surface subsidence for a given gas production case by pressure depletion from a methane hydrate reservoir in the PBU L-pad area. The development of this geomechanical model adheres to conservation principles, the effective stress law, and finite element method. Section II provides details of the geomechanical model, which includes field equations, constitutive relations, numerical procedures, the model regime, and input data.

Peak surface subsidence through time and contour maps showing surface subsidence and vertical displacement have been calculated using the geomechanical subsidence model for specific gas production cases by pressure depletion from a methane hydrate reservoir in the PBU L-pad area. Section III describes simulation results from the cases studied and Section IV presents conclusions drawn from this modeling study.

II. Full-Field, Three-Dimensional Subsidence Model

This study develops a full-field, 3D subsidence model that can be applied to various gas production cases by pressure depletion for methane hydrate reservoirs in the North Slope of Alaska, in particular the PBU L-pad area. The following section provides a detailed description of the model.

The Modeled Regime

Figure 2-1 (a) illustrates the modeled regime, which consists of reservoir, overburden, and underburden regions. The reservoir region of the full-field, 3D subsidence model (73 x 73 x 64 cells) includes the reservoir section of the PBU L-pad reservoir simulation model (see Appendix 1) with a mesh of 67 cells in the x-direction, 67 cells in the y-direction and 64 reservoir layers and the sideburden, as shown in Figure 2-1 (b). The

reservoir simulation model was created using the TOUGH+Hydrate reservoir simulator. The geological and geometric description of the 64 reservoir layers in the hydrate reservoir simulation model (67 x 67 x 64 cells) was shared by the subsidence model. The reservoir section of the subsidence model has the same geometric structure and mesh configuration (67 x 67 x 64 cells) and same porosity and pressure distributions as the TOUGH+Hydrate reservoir model.

The overburden region in the subsidence model was separated into four zones corresponding to four sets of material properties. The top zone was divided laterally into five layers, the next two zones were divided laterally into six layers for each zone, and the bottom zone was divided laterally into three layers between the bottom of the third zone and the top of the reservoir region. The underburden region was divided into two lateral layers between the bottom of the reservoir region and the bottom of the model regime. Thus, there were 73 x 73 x 20 cells for the overburden regions and 73 x 73 x 2 cells for the underburden regions.

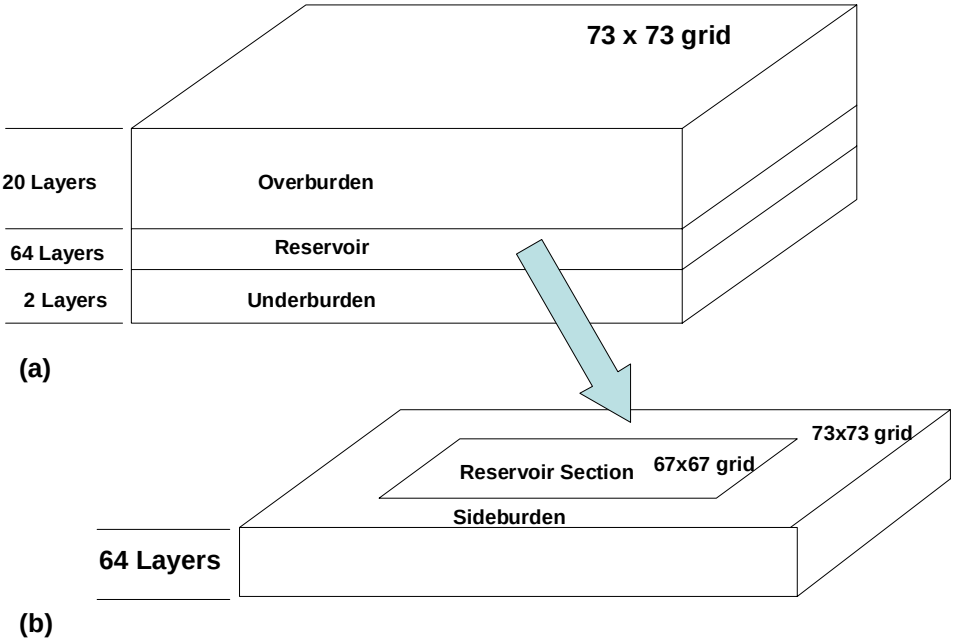

Figure. 2-1. Schematic of the modeled regime.

Governing Equations

The governing equations used for modeling the subsidence process in gas hydrate reservoirs were formulated based on the basic principles of the conservation of linear momentum and the effective stress law [1-3]. These equations are presented as follows:

For the reservoir:

$$\nabla \cdot \underset{\sim}{\sigma} + \rho \underset{\sim}{b} = 0 \quad (1)$$

$$\underset{\sim}{\sigma} = \underset{\sim}{\sigma}' - p\,\underset{\sim}{\delta} \quad (2)$$

For the overburden and underburden:

$$\nabla \cdot \underset{\sim}{\sigma} + \rho \underset{\sim}{b} = 0 \quad (3)$$

where $\underset{\sim}{\sigma}$ = solid total stress, $\underset{\sim}{\sigma}'$ = solid effective stress [3], $\underset{\sim}{b}$ = body force, p = pore pressure, ρ = solid bulk density, and $\underset{\sim}{\delta}$ = Kronecker delta. Note that the sign is positive for tension and negative for compression.

Supplementing Equations 1 to 3 with the appropriate constitutive equations for reservoir rock, overburden, and underburden, and reservoir pressure-time maps obtained from the given gas production case by pressure depletion in a methane hydrate reservoir, the full set of governing equations was derived as a system of partial differential equations and numerically solved for the solid-displacement distribution of the entire modeled regime. Surface subsidence was obtained through the solution of the solid-displacement distribution. The solution of the displacement field vector also allowed for the determination of stress and strain distributions within the reservoir, overburden, and underburden. The details of the modeling procedure are presented in References 1 and 2.

Constitutive Models

1. Reservoir Rock

The deformation behavior of hydrate reservoir rock is complicated because mechanical properties of hydrate reservoir rock change with hydrate saturation, while hydrate saturation decreases with time as gas production from the hydrate reservoir proceeds by pressure depletion. In general, the mechanical strength of reservoir rock with low hydrate saturation can be fivefold to sevenfold weaker than that with high hydrate saturation. To simplify the calculation procedure, in this study limiting cases were designed and investigated to obtain the range of predicted subsidence values for a given gas production case by pressure depletion in the methane hydrate reservoir. An isotropic, linear elastic constitutive model was applied for simulating the deformation behavior of the hydrate reservoir rock. Two mechanical properties for the linear elastic model are Young's modulus and Poisson's ratio. Generally, the deformation behavior of hydrate reservoir rock depends on its initial porosity, hydrate saturation, and loading conditions. Under a specified loading condition (hydrostatic or uniaxial strain), Young's modulus can be related to pore-volume rock compressibility, the initial porosity, and Poisson's ratio. With the initial porosity distribution and pore volume rock compressibility specified from the TOUGH+Hydrate reservoir model and an estimated average Poisson's ratio, Young's

modulus values for all the reservoir cells in the subsidence model were then determined from their corresponding values of rock compressibility and initial porosity. In this study, Young's modulus values determined from rock compressibility values used by the TOUGH+Hydrate reservoir model at initial porosity are designated as the base-case values, while one tenth of Young's modulus values of the base-case values are designated as the weakest-case values. Young's modulus with the base-case values is considered for a situation with high average hydrate saturation in the reservoir and Young's modulus with the weakest-case values is considered for a condition that the hydrate reservoir is nearly depleted with low average hydrate saturation.

2. Overburden and Underburden Rocks

Based on the reasonable assumption that no fluid drainage occurs in the overburden and underburden zones, the geomaterials in these zones are considered as single-phase solid materials. An isotropic, linear elastic constitutive model was used for both the overburden and underburden rocks. However, each zone is assigned different values of Young's modulus and Poisson's ratio. In addition, the overburden is further divided into a number of lateral layers and these layers are assigned a unique set of values for Young's modulus and Poisson's ratio that are estimated from well log data.

Numerical Procedures

1. Finite Element Discretization

The numerical procedure for solving the governing equations of the deformation process, described in Section II.B, requires pore pressure-time curves for all the reservoir cells in the subsidence model in order to compute effective stresses and rock deformation caused by changes in effective stress. These pore pressure-time maps were generally obtained from simulation runs conducted by reservoir engineers using the TOUGH+Hydrate reservoir model for different gas production cases by pressure depletion in a methane hydrate reservoir. The Galerkin finite element method [4] is used to discretize the governing equations for the subsidence model with the finite element mesh as shown in Figure 2-2. The finite element mesh of the model developed for this study has 458,294 elements (73 x 73 x 86). The 86 model layers consist of 20 layers in the overburden, 64 in the reservoir, and 2 in the underburden.

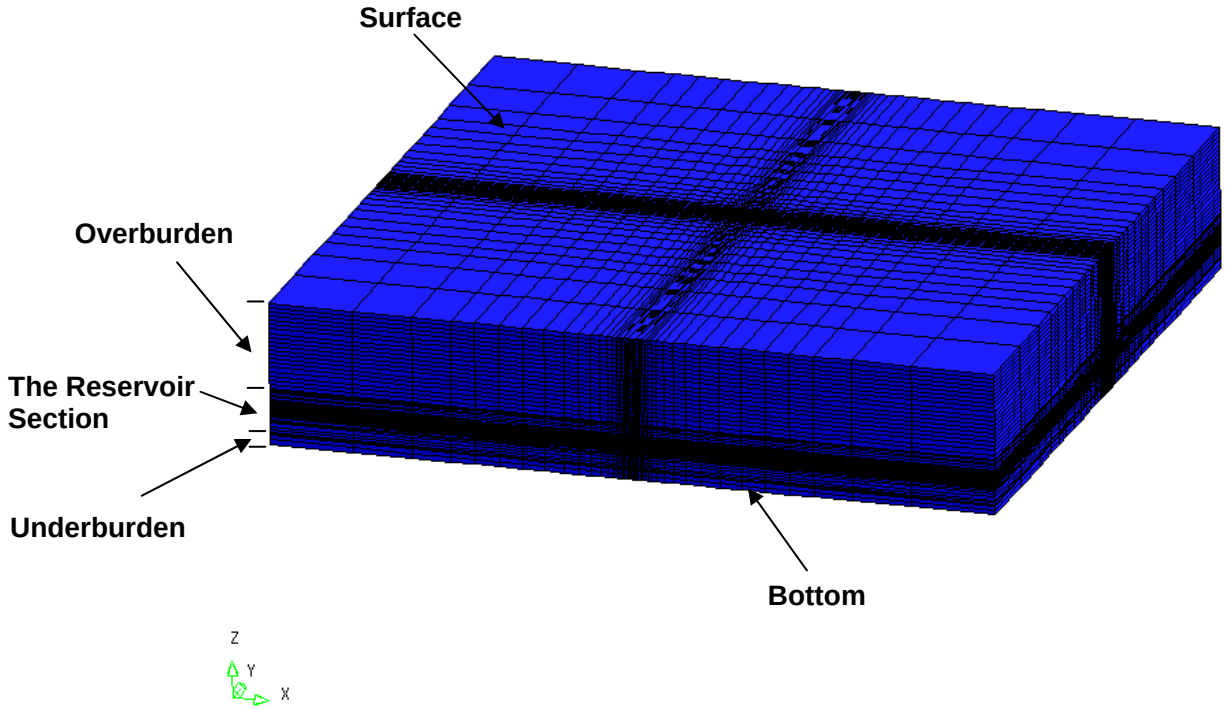

Figure 2-2: The finite element mesh for the full-field, 3D surface subsidence model.

2. Boundary Conditions

The boundary conditions applied for the finite element model assume no movement at the bottom of the underburden, nor is movement allowed at the external boundary of the model (the outside boundary of the modeled regime). As described in Section II.A, the subsidence model includes a large sideburden region surrounding the hydrate reservoir section in order to minimize the boundary effect on the calculation results from the subsidence model.

3. Solution of the Discretized System

The linear system of about 1,300,000 equations obtained from the finite element discretization and boundary conditions is solved by an iterative linear solver and provides the displacement field for the entire modeled regime. Based on the computed displacement field at each time step, the following information has been generated: simulation results of surface subsidence versus time curves; subsidence contour maps; vertical displacement contour maps; and stress and strain distributions.

Input Data

1. Mechanical and Physical Properties of the Reservoir Region

As described in Section II.A, the reservoir region consists of the reservoir section and the sideburden surrounding the reservoir section. The mechanical properties of the rock used in this study for the reservoir section are based on the values of pore volume rock compressibility used in the PBU L-pad TOUGH+Hydrate reservoir model, which are dependent on six rock types.

In the TOUGH+Hydrate reservoir model,

Rock type 1 (D Sand): $C_p = 12.0 \times 10^{-6}$ (4)
Rock type 2 (D Shale): $C_p = 17.0 \times 10^{-6}$ (5)
Rock type 3 (Upper C Sand): $C_p = 12.0 \times 10^{-6}$ (6)
Rock type 4 (Lower C Sand): $C_p = 11.0 \times 10^{-6}$ (7)
Rock type 5 (C Shale): $C_p = 16.0 \times 10^{-6}$ (8)
Rock type 6 (B Sand): $C_p = 21.0 \times 10^{-6}$ (9)

where C_p = pore-volume rock compressibility, psi^{-1}.

Young's modulus can be expressed by the equation:

$$E = 3(1 - 2\nu)/\varphi/C_p \quad (10)$$

where E = Young's modulus, psi; ν = Poisson's ratio; φ = initial porosity.

Substituting Eqs. 4 to 9 into Eq. 10, Young's modulus for reservoir cells associated with different rock types and initial porosity values in the subsidence model can be calculated by the equations:

Rock type 1 (D Sand): $E = (1 - 2\nu)/\varphi/ (12.0 \times 10^{-6})$ (11)
Rock type 2 (D Shale): $E = (1 - 2\nu)/\varphi/(17.0 \times 10^{-6})$ (12)
Rock type 3 (Upper C Sand): $E = (1 - 2\nu)/\varphi/(12.0 \times 10^{-6})$ (13)
Rock type 4 (Lower C Sand): $E = (1 - 2\nu)/\varphi/(11.0 \times 10^{-6})$ (14)
Rock type 5 (C Shale): $E = (1 - 2\nu)/\varphi/(16.\ 0 \times 10^{-6})$ (15)
Rock type 6 (B Sand): $E = (1 - 2\nu)/\varphi/ (21.0 \times 10^{-6})$ (16)

In this study, an average value of 0.35 for Poisson's ratio was assigned to all the cells in the reservoir section of the subsidence model. With Poisson's ratio specified at 0.35, Figure 2-3 shows Young's modulus used in the subsidence model for cells in the reservoir section as a function of their initial porosity values for different rock types. The initial porosity distribution in the reservoir section of the subsidence model is taken from the PBU L-pad TOUGH+Hydrate reservoir model.

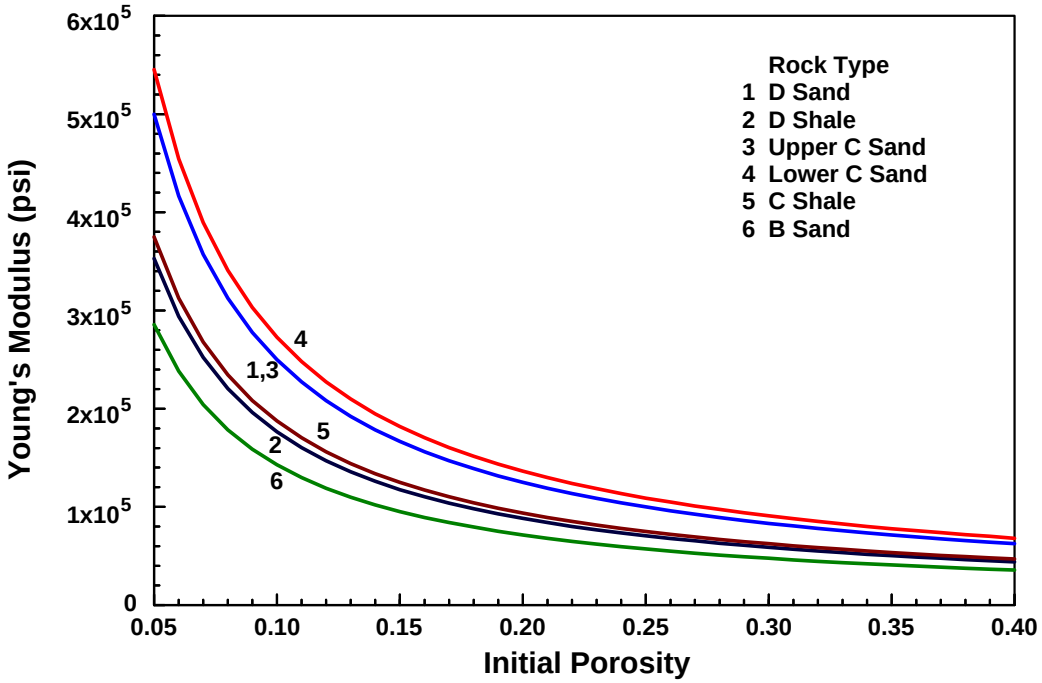

Figure. 2-3. Young's modulus in relation to initial porosity and rock type used for the subsidence model (The base-case values).

As discussed in Section II.C.1, the values of Young's modulus shown in Figure. 3 are considered as the base-case values for the six rock types and used to predict surface subsidence for the base cases in this study. Similarly, based on the discussion in Section II.C.1, the values of Young's modulus used for the weakest-case values to predict subsidence can be calculated from Equations 17 to 22, which are obtained by multiplying 0.1 to Equations 11 to 16 for six rock types, respectively:

Rock type 1 (D Sand): $E = 0.1x(1 - 2\nu)/\varphi/(12.0x10^{-6})$ (17)
Rock type 2 (D Shale): $E = 0.1x(1 - 2\nu)/\varphi/(17.0x10^{-6})$ (18)
Rock type 3 (Upper C Sand): $E = 0.1x(1 - 2\nu)/\varphi/(12.0x10^{-6})$ (19)
Rock type 4 (Lower C Sand): $E = 0.1x(1 - 2\nu)/\varphi/(11.0x10^{-6})$ (20)
Rock type 5 (C Shale): $E = 0.1x(1 - 2\nu)/\varphi/(16.\ 0x10^{-6})$ (21)
Rock type 6 (B Sand): $E = 0.1x(1 - 2\nu)/\varphi/(21.0x10^{-6})$ (22)

With the Poisson's ratio specified at 0.35, Figure 2-4 shows Young's modulus used for the weakest-case values for cells in the reservoir section as a function of their initial porosity values for different rock types in the subsidence model.

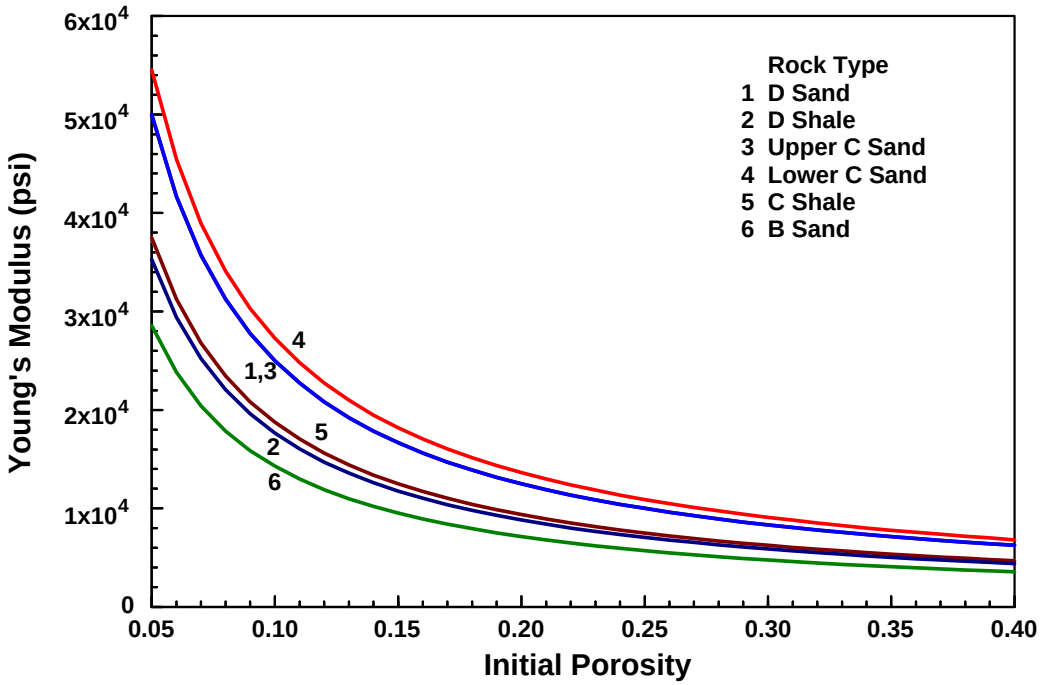

Figure. 2-4. Young's modulus in relation to initial porosity and rock type used for the subsidence model (weakest-case values).

The sideburden surrounding the reservoir section is divided into the same number of layers as the reservoir. Each sideburden layer is assigned the same values of bulk density, Young's modulus, and Poisson's ratio as those at the boundary of the reservoir section for the corresponding reservoir layer. In the subsidence model, the sideburden was treated as an isotropic, linear elastic material.

2. Mechanical and Physical Properties of the Overburden and the Underburden

The overburden of the subsidence model is treated as an isotropic, linear-elastic material. The overburden is divided laterally into four zones; the uniform properties assigned for each zone are presented in Table 2-1. The data in Table 1 have been estimated from well log data. In the finite element model, each zone is divided further into several lateral layers for the purpose of refining the mesh. In the subsidence model, lateral layer 1 is the top layer with surface and lateral layer 20 is the bottom layer adjacent to the top of the reservoir model.

Table 2-1 – Overburden properties used in the subsidence model

Zone	Layer type	Depth interval (ft)	Lateral layers	Bulk density (g/cc)	Young's modulus (psi)	Poisson's ratio
1	Permafrost	0 - 500	5	1.82	$0.5x10^5$	0.44
2	Permafrost	500 - 1100	6	1.92	$1.0x10^5$	0.40
3	Bottom of permafrost	1100 – 1700	6	1.96	$1.1x10^5$	0.40
4	Sands and shales	1700 – the top of reservoir model	3	1.99	$1.8x10^5$	0.35

The zone of rock below the reservoir (the underburden) is treated as an isotropic, linear-elastic material. The underburden is assigned a bulk density of 2.32 g/cc, a Young's modulus of $3.6x10^5$ psi, and a Poisson's ratio of 0.33. In general, subsidence predictions are not very sensitive to these underburden property values when they are estimated reasonably.

3. Geological and Geometric Descriptions

The geological and geometric descriptions of the reservoir section used to develop the 3D subsidence model for the PBU L-pad area are based on the geological and geometric descriptions from the PBU L-pad TOUGH+Hydrate reservoir model (a 67 x 67 x 64 cell model). Information from the PBU L-pad TOUGH+Hydrate reservoir model, including porosity distributions for the 64 reservoir layers, rock type distributions for the 64 reservoir layers, geometric features of the layers, and the mesh configuration, are employed to construct the reservoir section of the subsidence model. Note that, since the geological and geometric descriptions of the subsidence model are coupled with those of the reservoir model, reconstructing the subsidence model is required whenever the reservoir model is expanded and refined.

For this study, both AIM and Archie methods are used to generate the initial saturation distribution (methane hydrate, water, gas, and ice saturations) in the reservoir section for the TOUGH+Hydrate reservoir model (See Appendix 1). Two reservoir models developed by using the AIM and Archie methods are designated as the AIM model and the Archie model in this report. Because of the difference in distributions of initial saturations, simulation results from the two reservoir models are different even for a give production case with the same pressure depletion condition.

In Section II.E.1, Eq. 10 shows that variation of Young's modulus of reservoir rock in the PBU L-pad area is related to initial porosity distribution in each reservoir layer. Initial porosity distributions for selected reservoir layers (Layers 18, 24, and 29) in the upper C sand formation are illustrated in Figures 2-5, 2-6, and 2-7, respectively. Note that the AIM model and the Archie model have the same initial porosity distribution. Figures 2-

4, 2-5, and 2-6 indicate that main initial porosity values range from 0.3 to 0.4 in layers 18, 24, and 29.

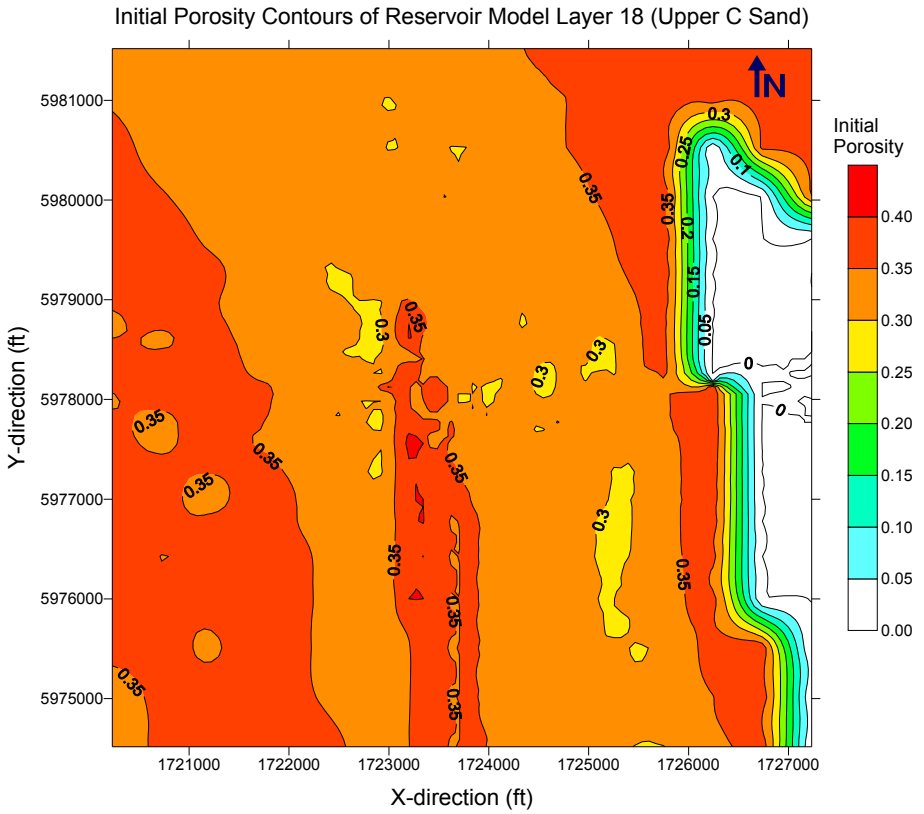

Figure 2-5: Initial porosity distribution in reservoir model layer 18 (Upper C sand).

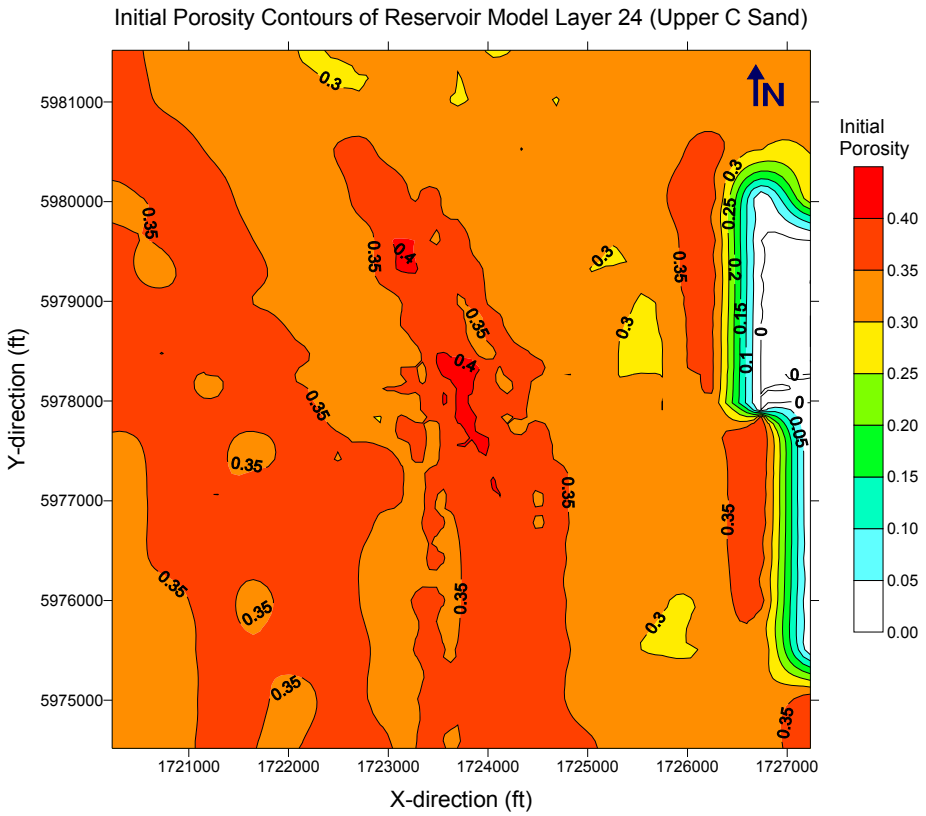

Figure 2-6: Initial porosity distribution in reservoir model layer 24 (upper C sand).

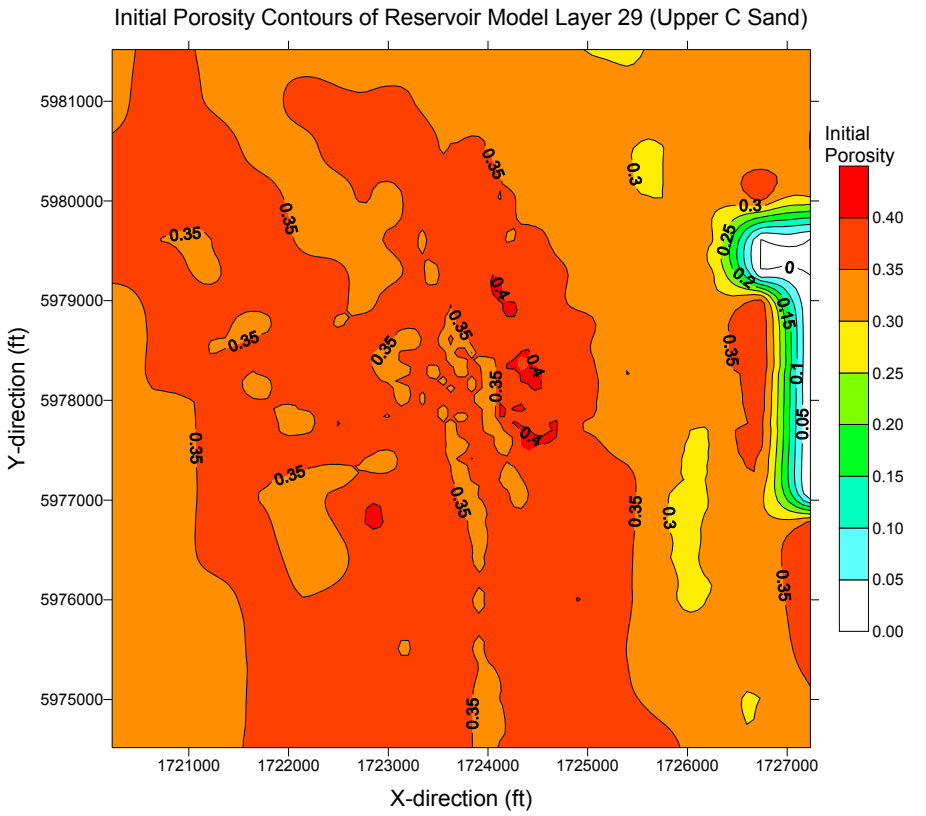

Figure 2-7: Initial initial porosity distribution in reservoir model layer 29 (Upper C sand).

4. Reservoir Pressure Maps

This study examines a 2-year gas production case by pressure depletion from the methane hydrate reservoir to calculate surface subsidence in the PBU L-pad area on the North Slope of Alaska. The general characteristics of the gas production case by pressure depletion are illustrated by contour maps showing pressure distribution in the producing formation at different producing times, shown in Figures 2-8 to 2-12. Figures 2-8 to 2-12 show that at any given time, the AIM model yields a larger pressure depletion area than the Archie model for the given gas production case. The pressure contours presented in Figures 2-8 to 2-12 clearly illustrate that the size of the pressure depletion area increase with time for both AIM and Archie models as more methane hydrate disassociated in the hydrate reservoir by pressure depletion. In this study, for the given gas production case, a decrease in reservoir pressure will result in an increase in effective stress to compact the reservoir rock. The compaction of reservoir rock induces overburden downward movement transferred to the surface as surface subsidence. Reservoir pressure versus time curves used in surface subsidence prediction for this modeling study were obtained from the result of TOUGH+Hydrate reservoir simulation by either the AIM model or the Archie model (Appendix 1). Based on the procedure described in Section II.D, a total of 287,296 separate pressure-time curves obtained from the reservoir model have been used in the 3D subsidence model for a given gas production case.

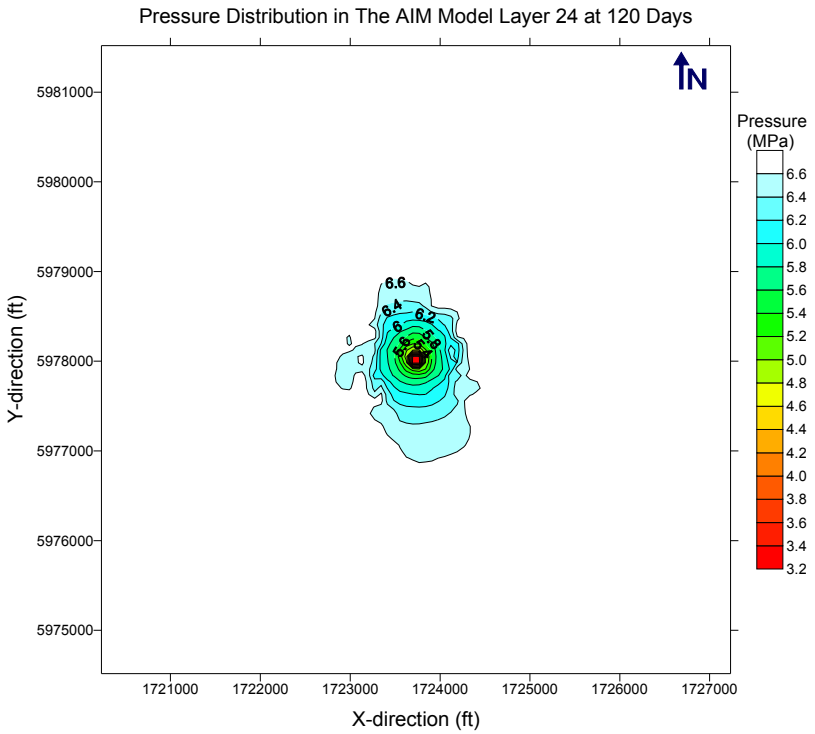

(a) The AIM model

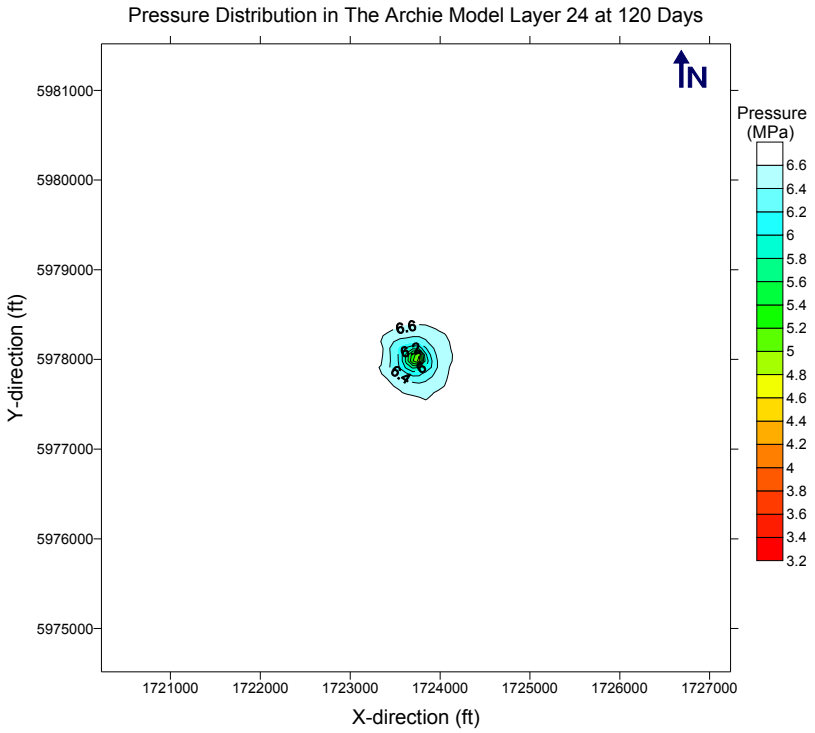

(b) The Archie model

Figure 2-8: Pressure distribution in reservoir layer 24 at producing time 120 days for the gas production case by pressure depletion studied (AIM model vs. Archie model).

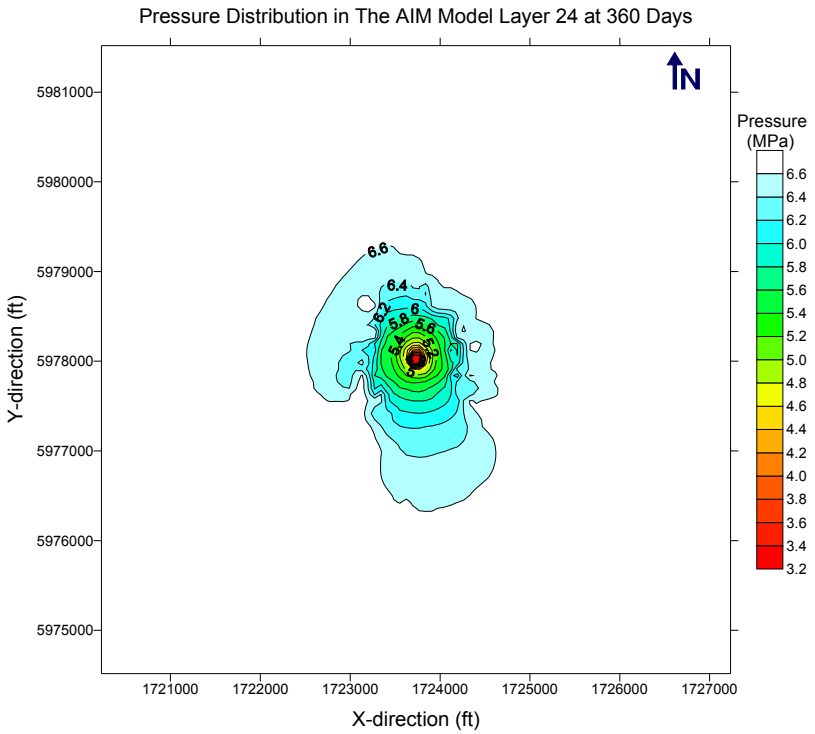

(a) The AIM model

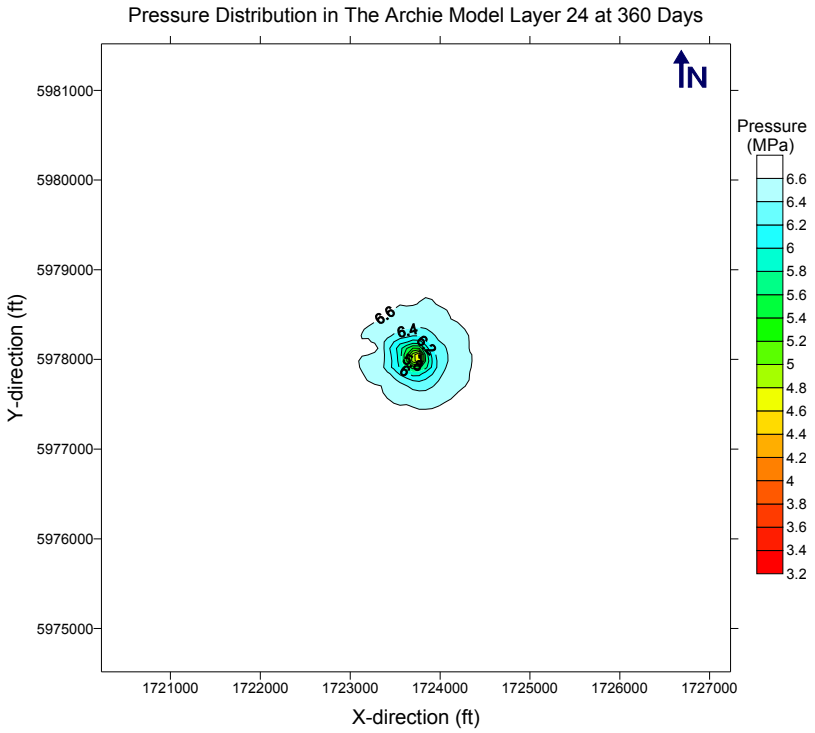

(b) The Archie model

Figure. 2-9: Pressure distribution in reservoir layer 24 at producing time 360 days for the gas production case by pressure depletion studied (AIM model vs. Archie model).

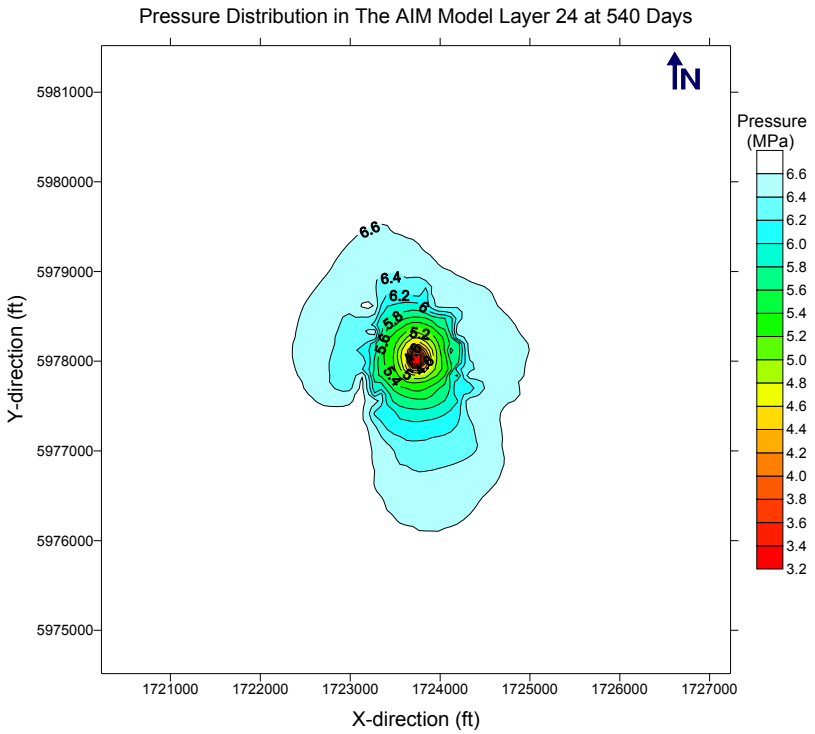

(a) The AIM model

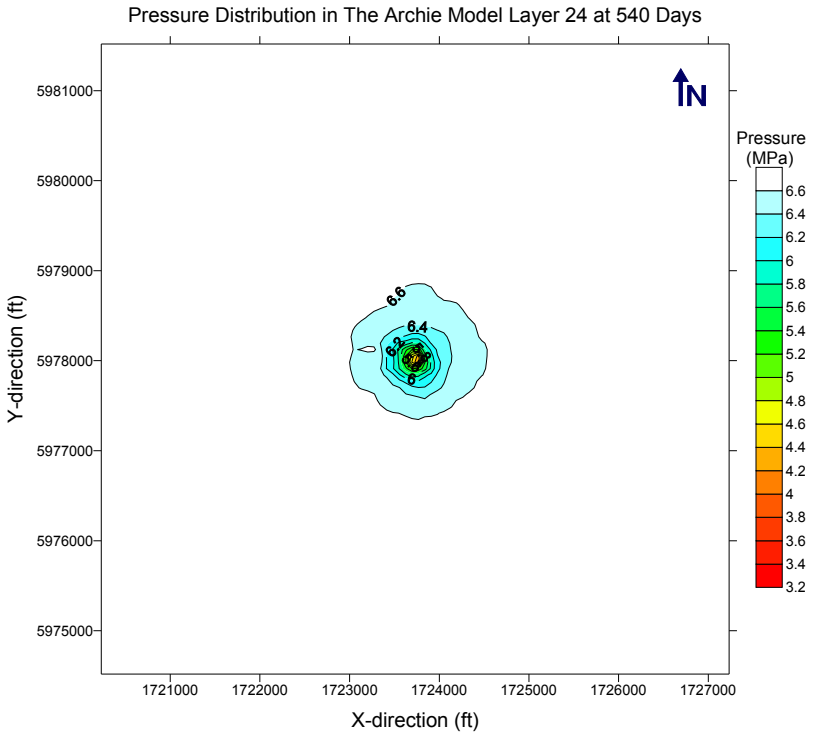

(b) The Archie model

Figure 2-10: Pressure distribution in reservoir layer 24 at producing time 540 days for the gas production case by pressure depletion studied (AIM model vs. Archie model).

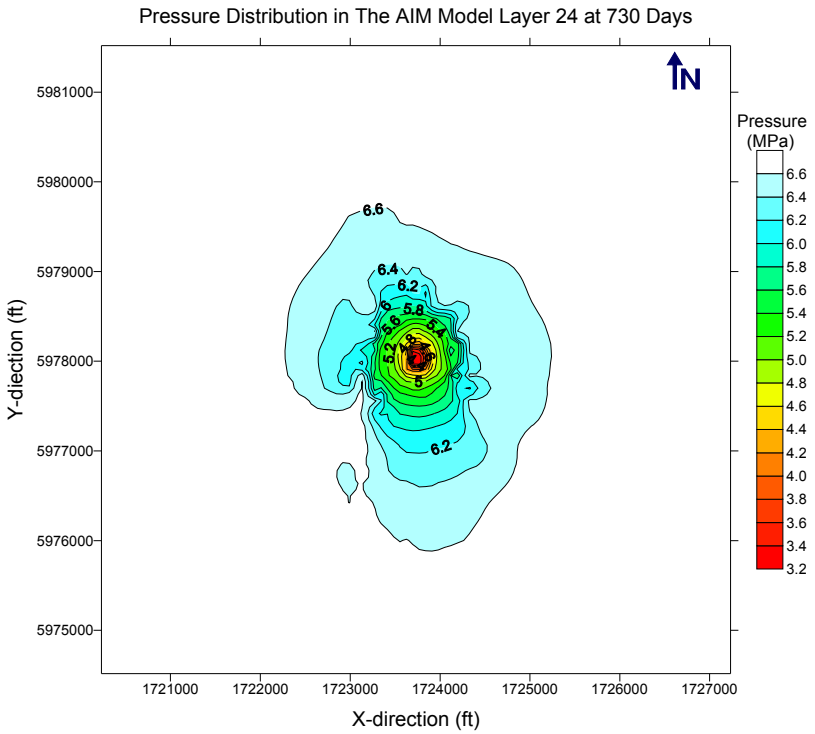

(a) The AIM model

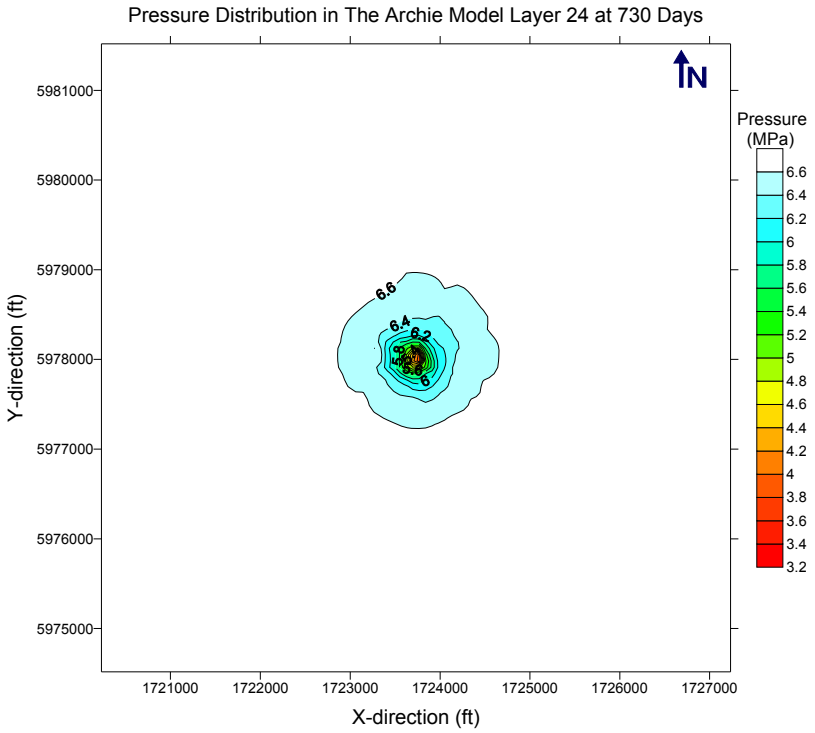

(b) The Archie model

Figure 2-11: Pressure distribution in reservoir layer 24 at producing time 730 days for the gas production case by pressure depletion studied (AIM model vs. Archie model).

III. SIMULATION RESULTS

A. Simulation Cases

Using the developed geoemchanics finite element model, surface subsidence predictions are performed for the given gas production scenario by pressure depletion from the methane hydrate reservoir in the PBU L-pad area in the North Slope of Alaska. As discussed in Section II.C.1, mechanical strength of hydrate reservoir rock decreases with a decrease in hydrate saturation during gas production from the methane hydrate reservoir. Six simulation runs including the base case, the pessimistic case, and the worst case for both the AIM and Archie models have been completed to evaluate the impact of gas production by pressure depletion from the methane hydrate reservoir on surface subsidence at the PBU L-pad area.

Table 2-2 presents the six runs studied. The base case uses Equations 11 to 16 to compute Young's moduli (the base-case values) for six rock types in the reservoir, while .the worst case uses Equations 17 to 22 to calculate Young's moduli (the weakest-case values) that are 10 times weaker than those of the base case. The pessimistic case used Young's moduli of the weakest-case values for rock type 3 (upper C sand) only and used Young's moduli of the base-case values for the rest of 5 rock types. The Upper C Sand is the main producing zone for these gas-production-via-depressurization studies. Thus, in this study the pessimistic case can be considered as the expected worst case for subsidence prediction, while the worst case is the unlikely worst case that gives severe subsidence prediction.

Table 2-2 – Description of six simulation runs investigated

Run	Case	Reservoir model	Young's modulus	Rock type applied
1	Base	AIM	Base-case values	1 to 6
2	Base	Archie	Base-case values	1 to 6
3	Pessimistic	AIM	Weakest-case values	3 (upper C sand)
			Base-case values	1, 2, 4, 5, and 6
4	Pessimistic	Archie	Weakest-case values	3 (upper C sand)
			Base-case values	1, 2, 4, 5, and 6
5	Worst	AIM	Weakest-case values	1 to 6
6	Worst	Archie	Weakest-case values	1 to 6

The simulation results of the six runs obtained for the given methane gas production case are presented in the following sections.

B. Surface Subsidence

Figure 2-12 shows peak surface subsidence versus time curves calculated by using the AIM model for the base case, the pessimistic case, and the worst case based on the given gas production case by depressurization in the methane hydrate reservoir. In Figure 2-12, the simulation results show that at producing time 730 days, the peak subsidence for the

base case, the pessimistic case, and the worst case is about 0.011, 0.073, and 0.118 feet (0.3, 2.2, 3.6 cm), respectively. Similarly, Figure 2-13 presents peak surface subsidence versus time curves calculated by using the Archie model for the three cases. As shown in Figure 13, the peak subsidence at producing time 730 days is about 0.006, 0.026, and 0.067 feet (0.2, 0.8, 2.0 cm) for the base case, the pessimistic case, and the worst case, respectively.

Predicted peak subsidence through time for the base case, the pessimistic case, and the worst case are compared between the AIM model and the Archie model in Figure 2-14, 2-15, and 2-16, respectively. Figures 2-14 to 2-16 clearly demonstrate that the predicted peak subsidence in the PBU L-pad area is strongly influenced by the method used for estimating the initial hydrate saturation in the methane hydrate reservoir. The results in Figures 2-14 to 2-16 show that the AIM model always predicts greater peak subsidence than the Archie model for the three cases studied because for the given gas production gas, at any given time the AIM model resulted in large pressure depletion area than the Archie model as shown in Figures 2-8 to 2-12.

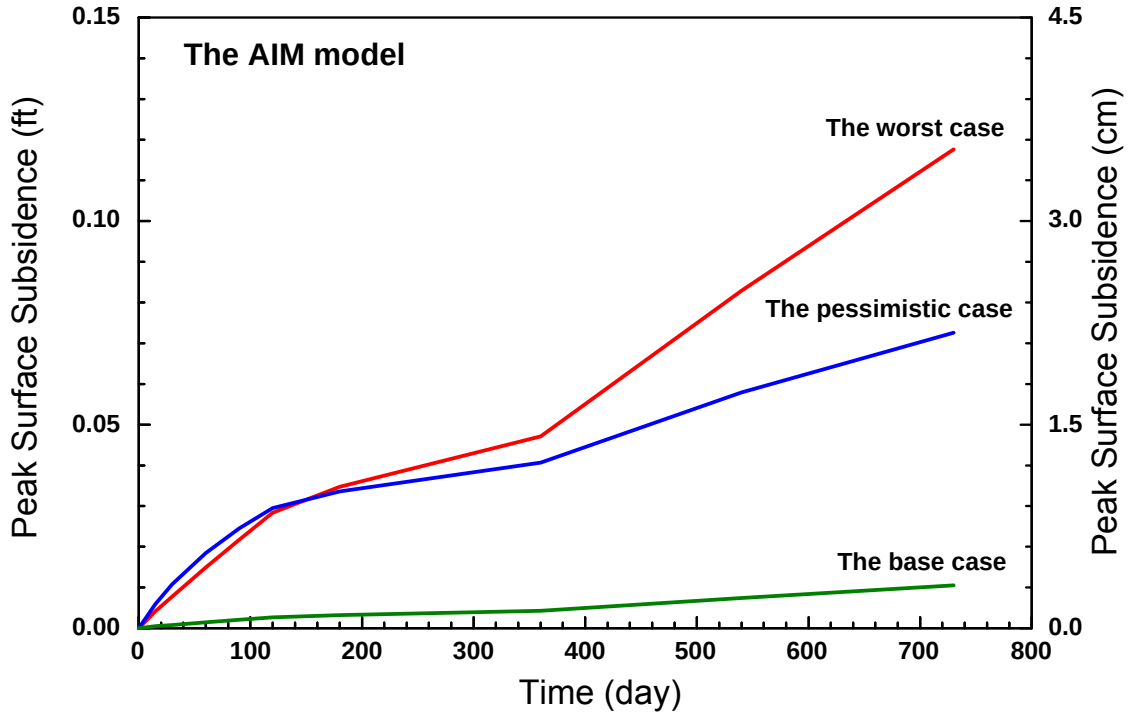

Figure 2-12: Peak subsidence prediction through time using the AIM model for three different cases in the PBU L-pad area.

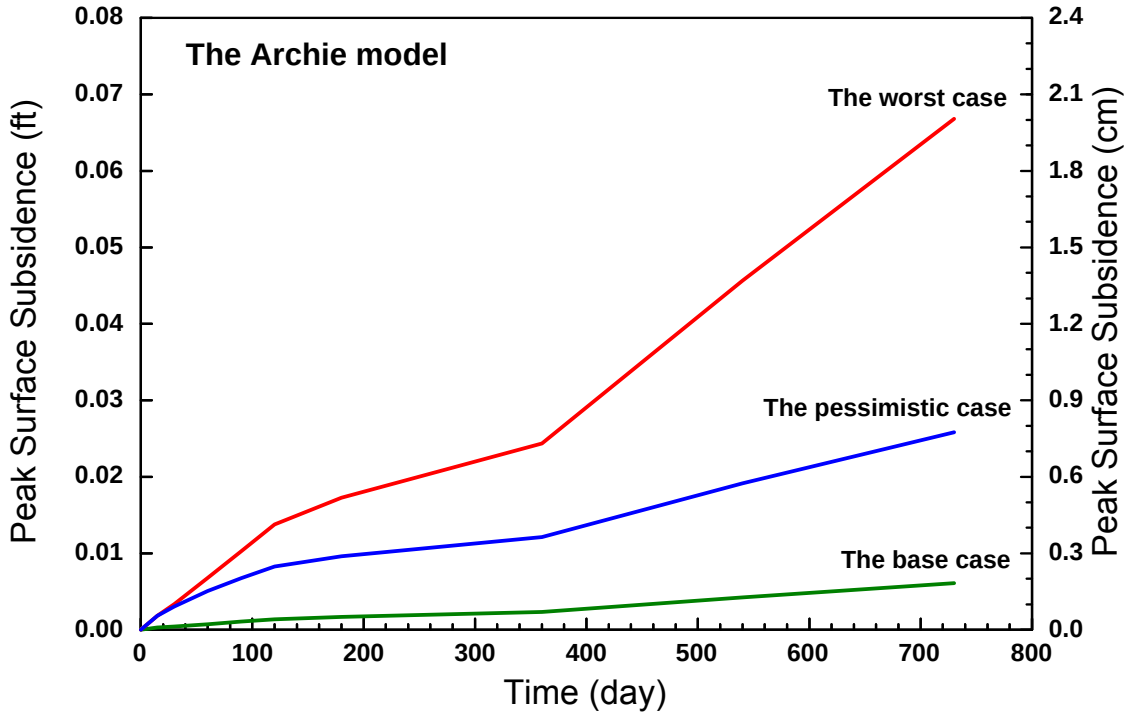

Figure 2-13: Peak subsidence prediction through time using the Archie model for three different cases in the PBU L-pad area.

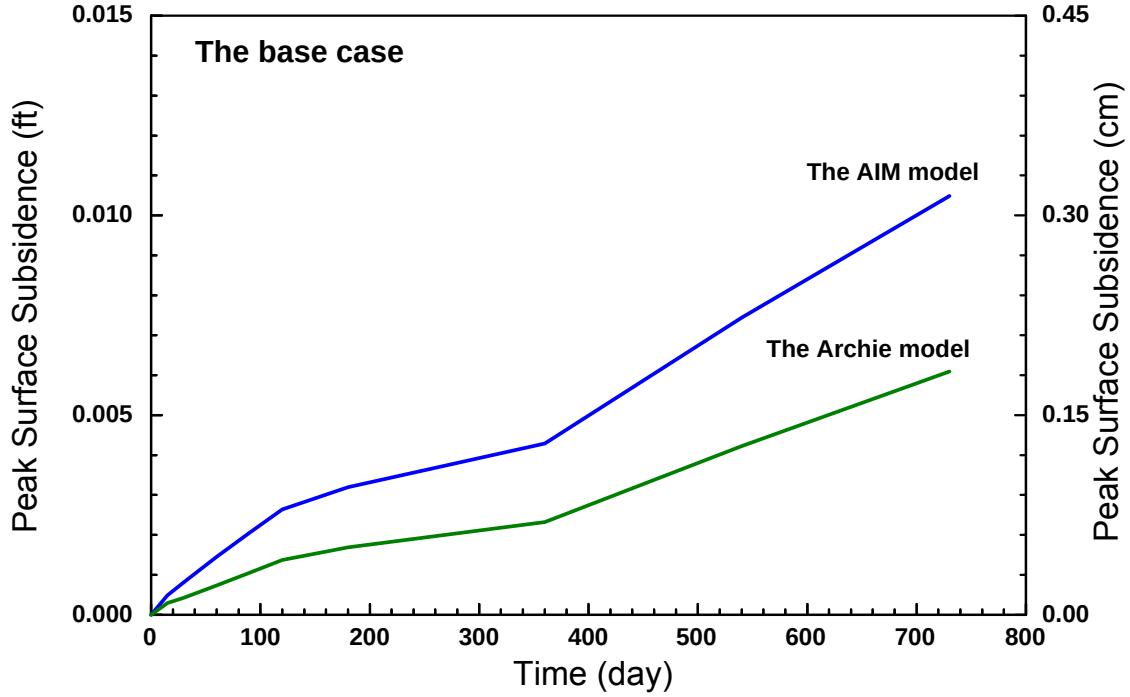

Figure 2-14: Comparison of peak subsidence prediction through time for the base case in the PBU L-pad area (AIM model vs. Archie model).

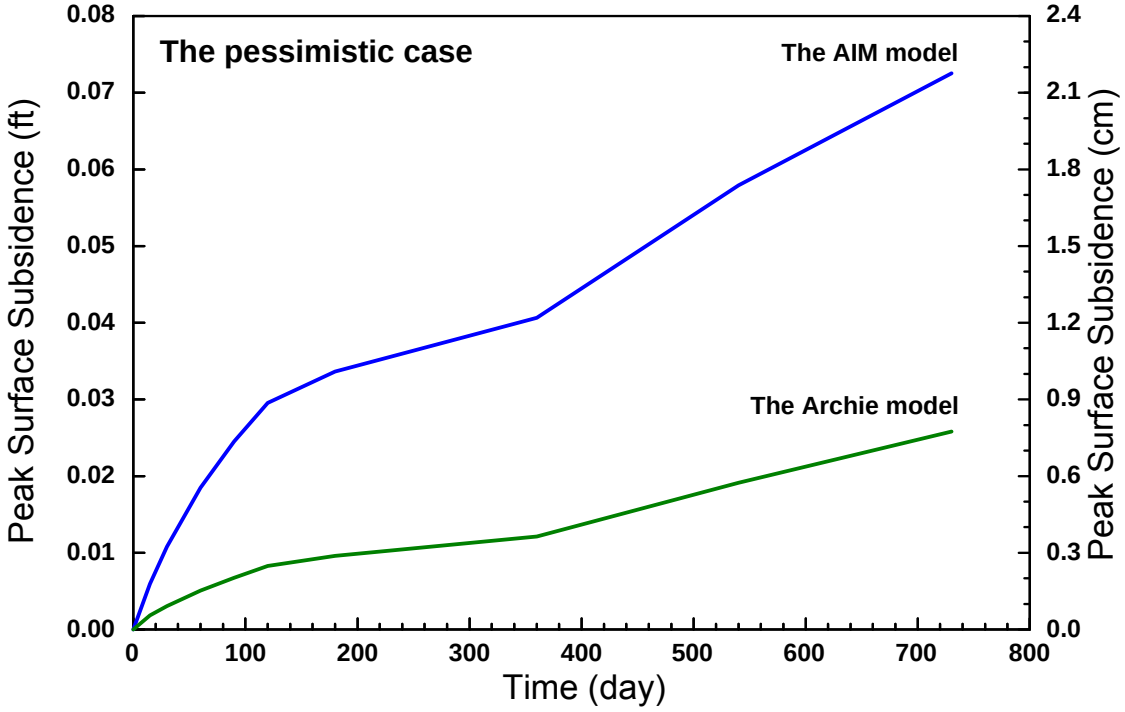

Figure 2-15: Comparison of peak subsidence prediction through time for the pessimistic case in the PBU L-pad area (AIM model vs. Archie model).

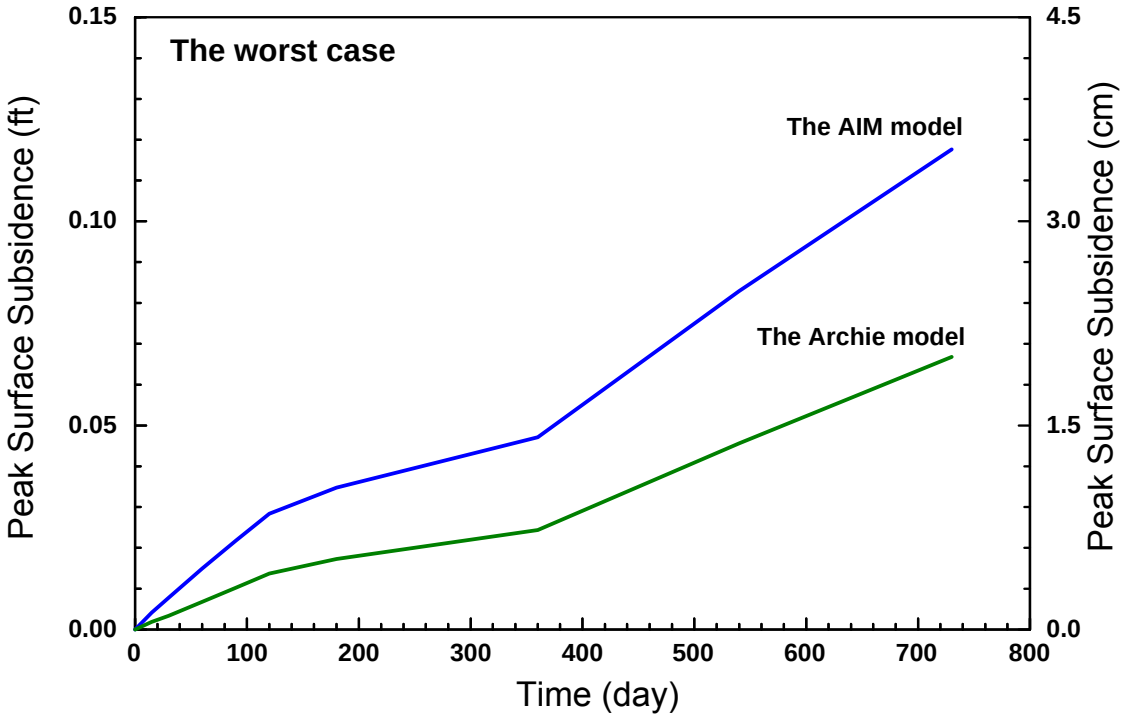

Figure 2-16: Comparison of peak subsidence prediction through time for the worst case in the PBU L-pad area (AIM model vs. Archie model).

Comparison of predicted peak surface subsidence values among these simulation cases at different producing times is summarized in Table 3. The results in Table 3 indicate that depending upon the simulation case studied, at producing time 730 days predicted peak subsidence in the PBU L-pad area ranges from 0.0061 to 0.1176 feet. The base case using the Archie model gives the lowest peak subsidence 0.0061 ft and the worst case using the AIM model predicts the highest peak subsidence 0.1176 ft.

Table 2-3 – Predicted peak surface subsidence for different simulation cases

Run	Case	Reservoir model	Peak surface subsidence (ft)		
			360 days	540 days	730 days
1	Base	AIM	0.0043	0.0074	0.0105
2	Base	Archie	0.0023	0.0042	0.0061
3	Pessimistic	AIM	0.0407	0.0579	0.0725
4	Pessimistic	Archie	0.0121	0.0191	0.0258
5	Worst	AIM	0.0471	0.0829	0.1176
6	Worst	Archie	0.0244	0.0456	0.0668

C. Surface Subsidence Contour Maps

Figures 2-17 through 2-19 present surface subsidence contour plots of the gas production case overlaid with wells locations at surface (blue circles) and surface locations of proposed wells for gas production from the hydrate reservoir (green circles) for the base case, the pessimistic case, and the worst case at producing time 730 days. As expected, these contour plots clearly show that the AIM model gives greater calculated surface subsidence than the Archie model. Figure 2-17 shows that for the base case, surface subsidence induced by pressure depletion from the methane hydrate reservoir is negligible for the given gas production case in the PBU L-pad area. For the pessimistic case, the results in Figure 2-18 show that the maximum surface subsidence is not greater than 0.073 ft which is a small value. Thus, for the pessimistic case, predicted peak surface subsidence caused by pressure depletion in the methane hydrate reservoir is not significant at the PBU L-pad area. Figure 19 yields similar findings that for the worst case, the maximum surface subsidence is about 0.12 feet for the given methane hydrate production case at the PBU L-pad area. Predicted surface subsidence of 0.12 feet from the worst case is still a small value and also the worst case designed in this study is an unlikely case for a methane hydrate reservoir with severely weak mechanical properties, as described in Section III.A.

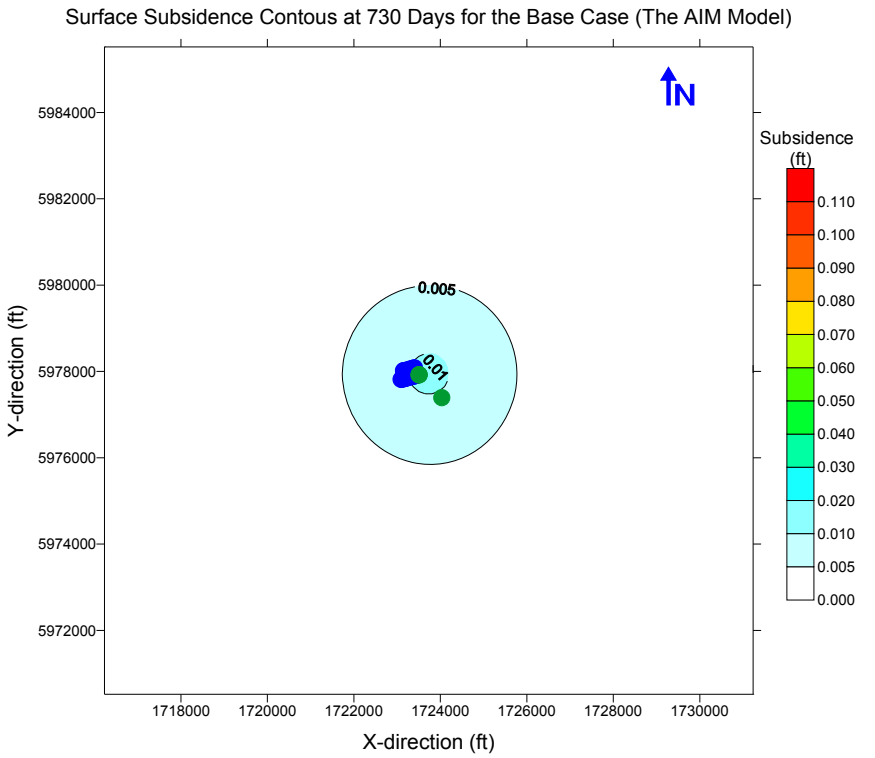

(a) The AIM model

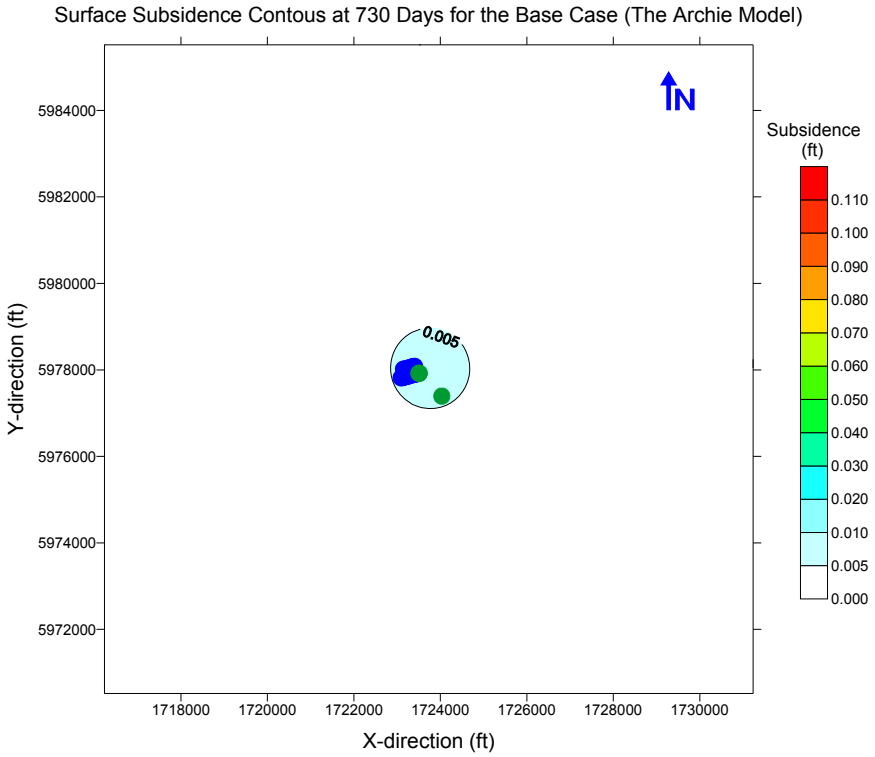

(b) The Archie model

Figure 2-17: Surface subsidence at 730 days for the base case in the PBU L-pad area (AIM model vs. Archie model).

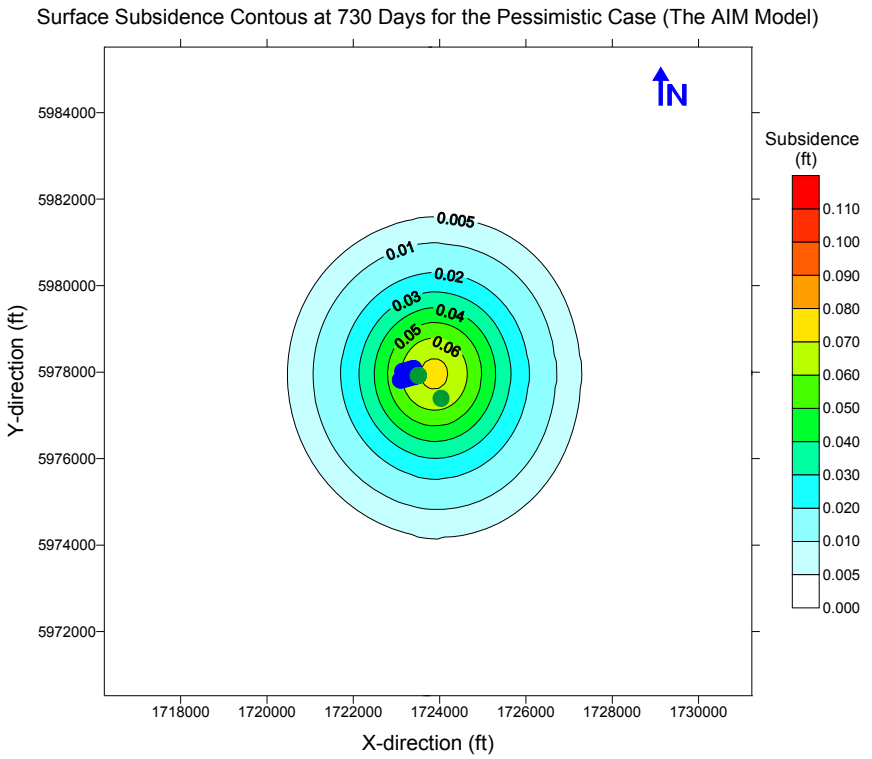

(a) The AIM model

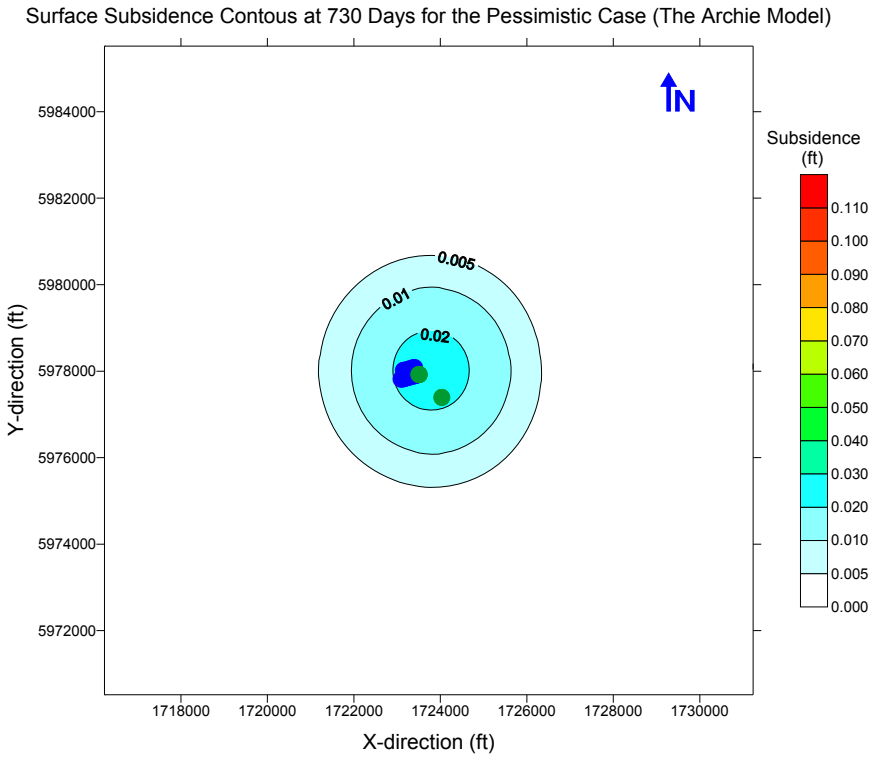

(b) The Archie model

Figure 2-18: Contour maps showing surface subsidence at 730 days for the pessimistic case in the PBU L-pad area (AIM model vs. Archie model).

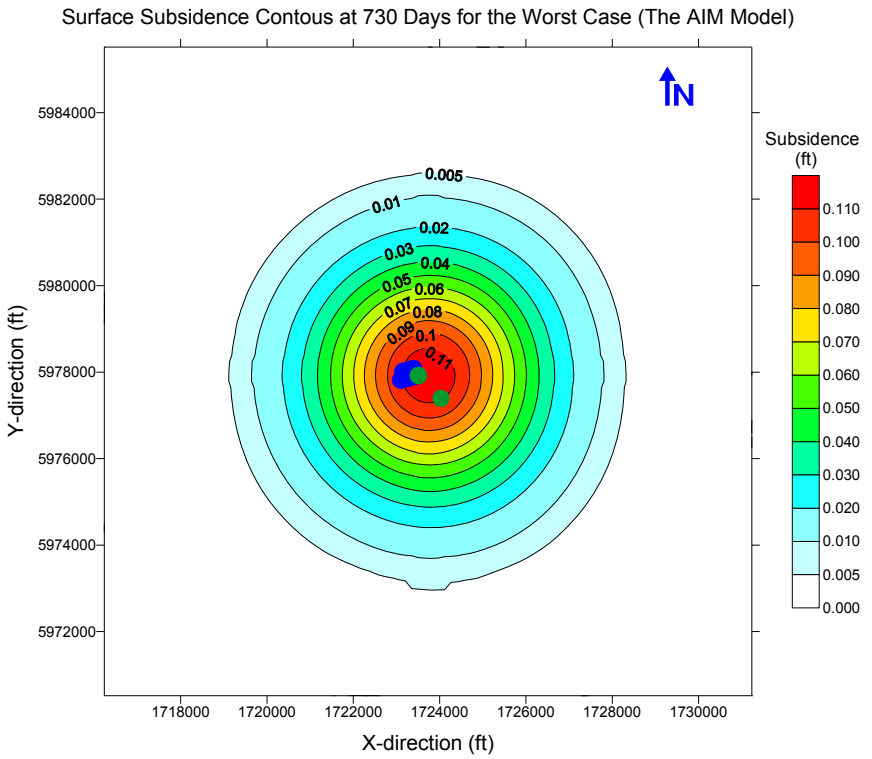

(a) The AIM model

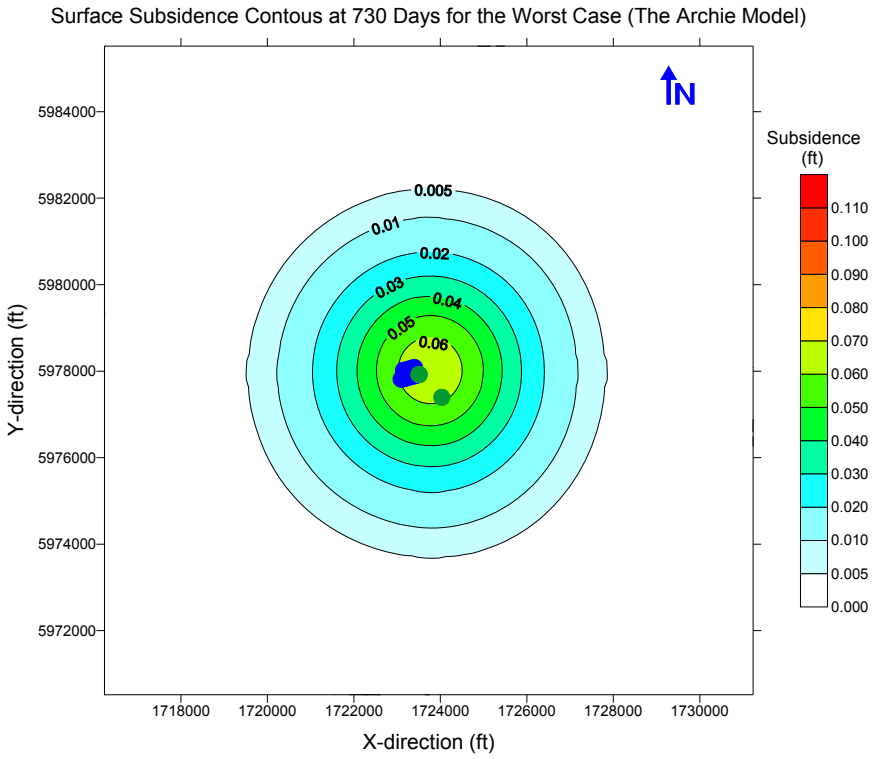

(b) The Archie model

Figure 2-19: Contour maps showing surface subsidence at 730 days for the worst case in the PBU L-pad area (AIM model vs. Archie model).

D. Vertical Displacement Contour Maps

Figures 2-20 through 2-22 present vertical displacement contour plots on the cross-section in the East-West cut through the center of the modeled domain for the base case, the pessimistic case, and the worst case, respectively. The positive contour value denotes the downward vertical displacement, while the negative contour value is for the upward vertical displacement. These contour plots indicate that vertical displacement in the overburden increases with depth until it reaches the top of the pressure depletion layer in the Upper C Sand. The upward displacement has large magnitude values near the bottom of the pressure depletion layer in the Upper C Sand and decreases with depth toward the underburden.

Again, at the same depth the AIM model predicts greater vertical displacements than the Archie model. For the worst case using the AIM model, the maximum downward vertical displacement is about 0.25 ft at a depth of about 2000 ft and the maximum upward vertical displacement in magnitude is about -0.30 ft at a depth of about 2200 ft.

Figures 2-23 through 2-25 present vertical displacement contour plots on the cross-section in the North-South cut through the center of the modeled domain for the base case, the pessimistic case, and the worst case, respectively. Contour plots in Figures 2-23 to 2-25 are similar to the plots in Figs. 2-20 to 2-22 for the cases studied. For the cases studied, the downward vertical displacement increases with depth in the overburden and the upward vertical displacement decreases with depth in the underburden. For the worst case using the AIM model, the maximum downward vertical displacement is about 0.25 ft at depth about 2000 ft, while the maximum upward vertical displacement is about 0.3 ft at depth about 2200 ft.

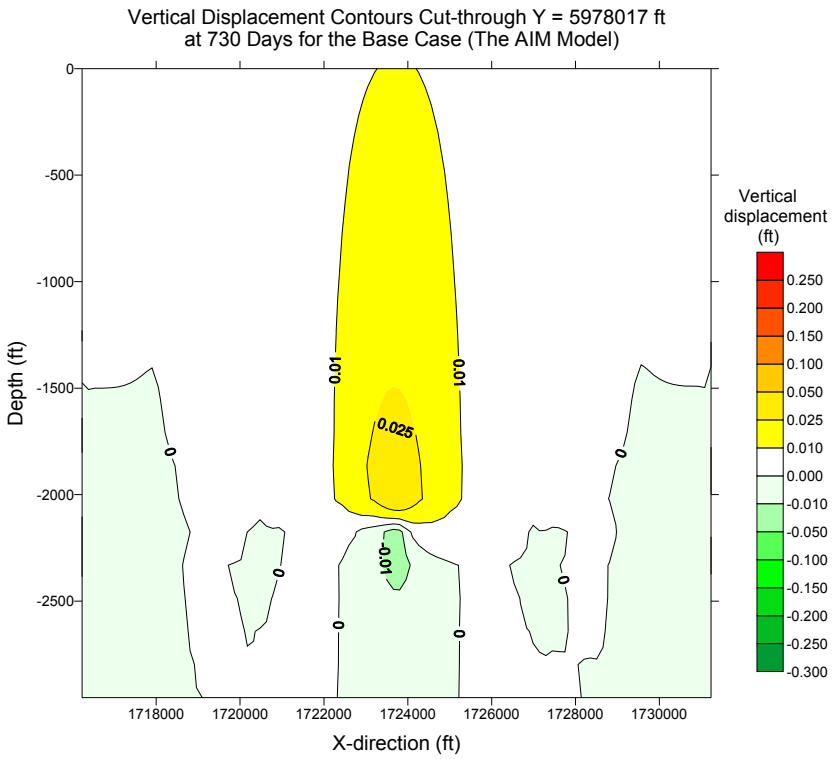

(a) The AIM model

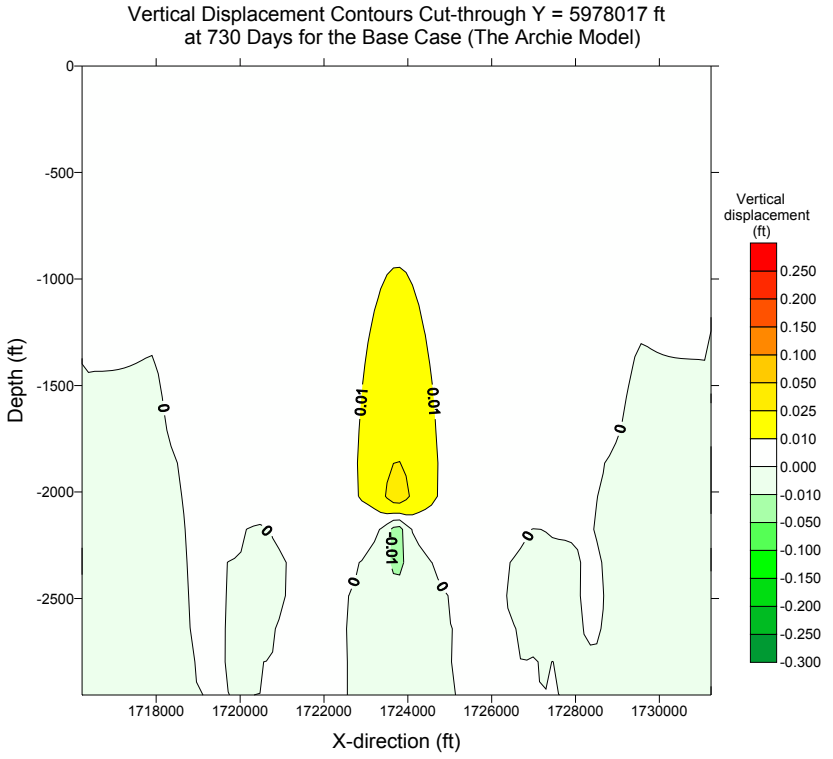

(b) The Archie model

Figure 2-20: Vertical displacements cut-through Y = 5978017 ft at 730 days for the base case at the PBU L-pad area (AIM model vs. Archie model).

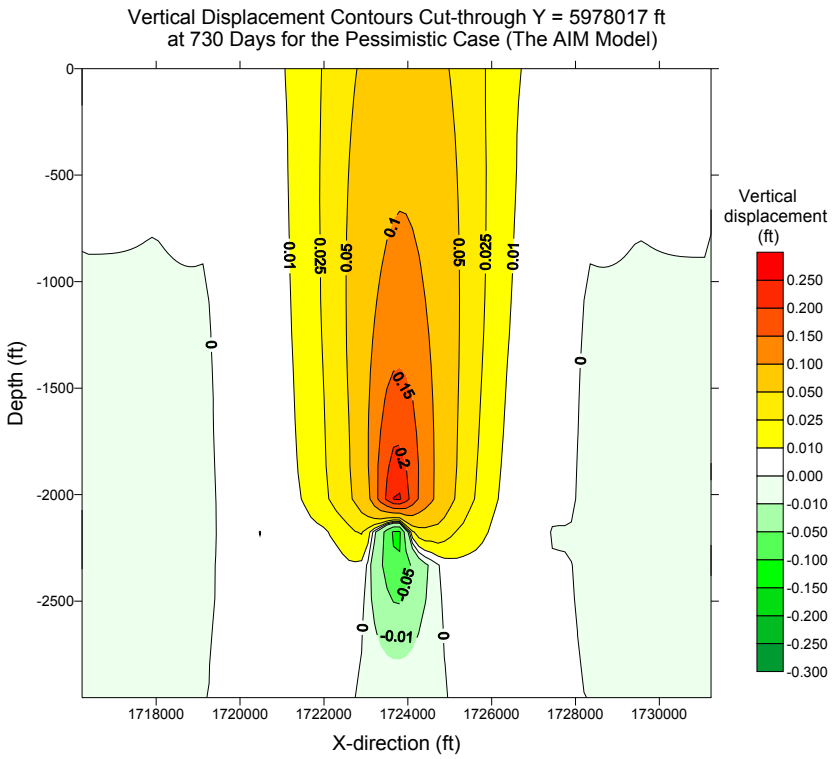

(a) The AIM model

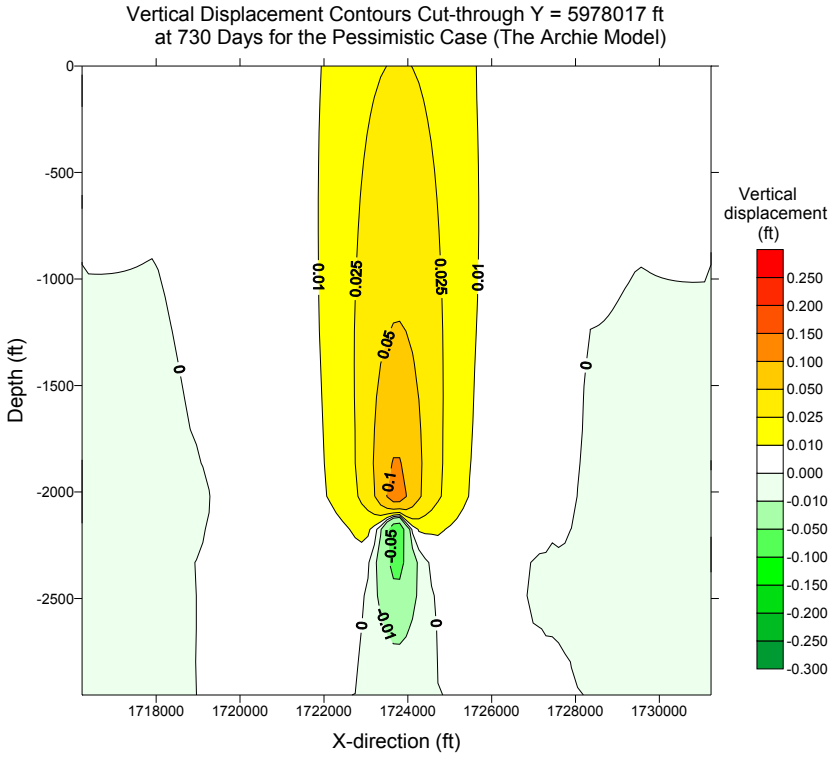

(b) The Archie model

Figure 2-21: Vertical displacements cut-through Y = 5978017 ft at 730 days for the pessimistic case at the PBU L-pad area (AIM model vs. Archie model).

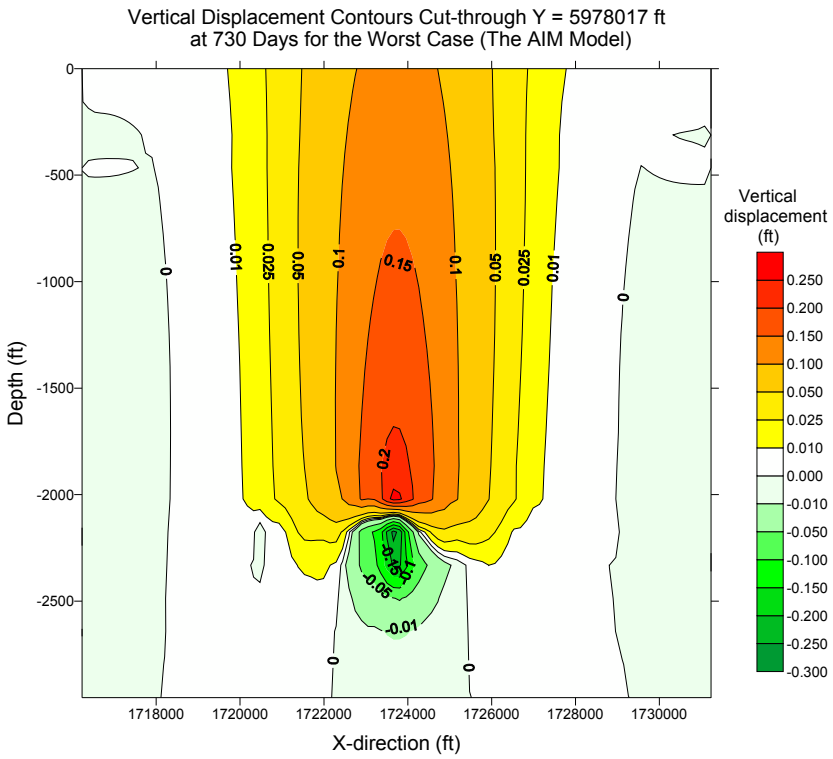

(a) The AIM model

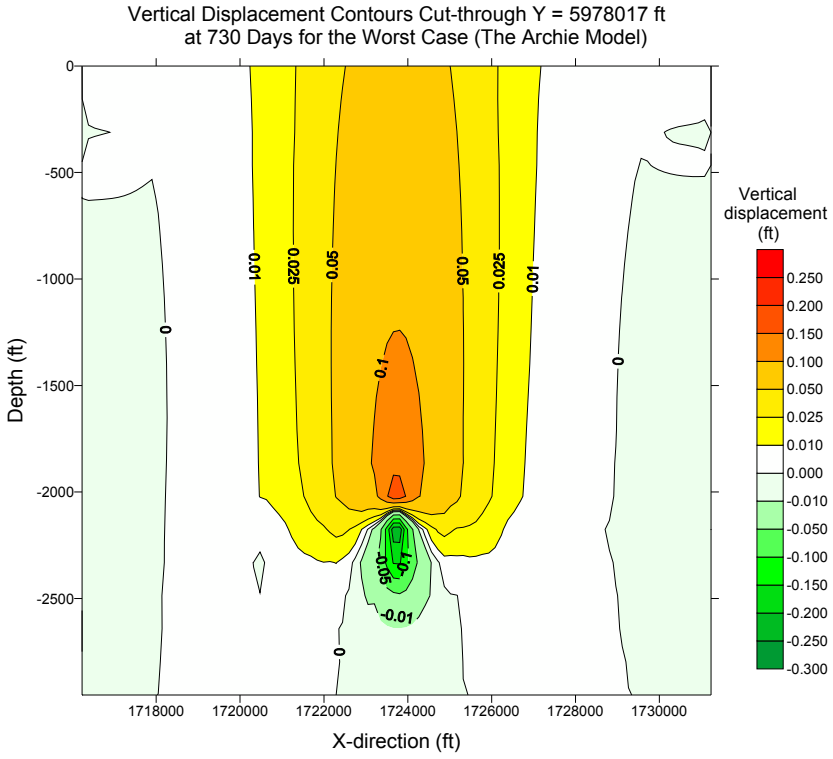

(b) The Archie model

Figure 2-22: Vertical displacements cut-through Y = 5978017 ft at 730 days for the worst case at the PBU L-pad area (AIM model vs. Archie model).

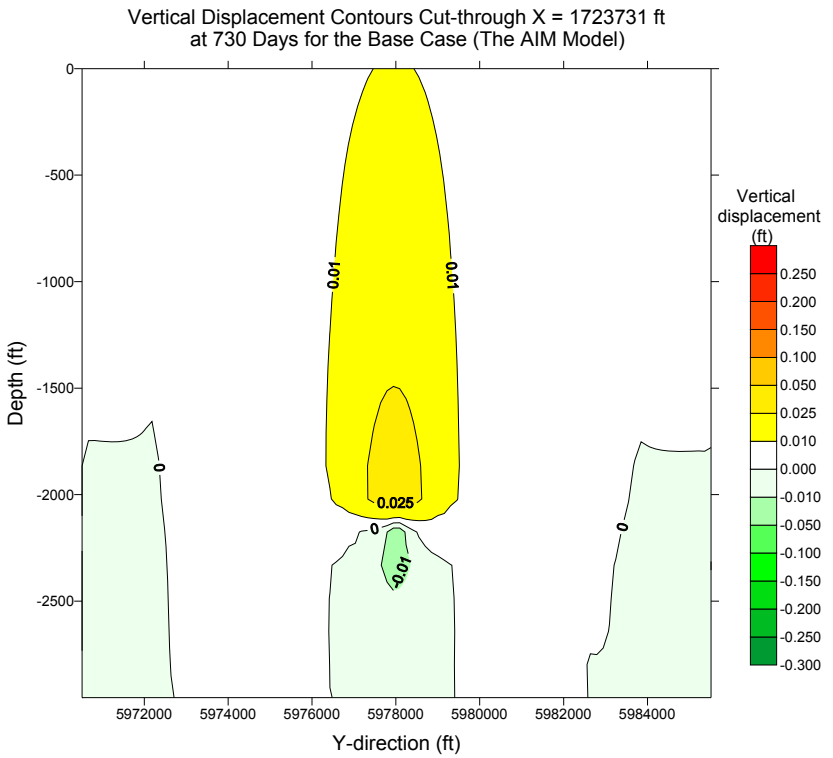

(a) The AIM model

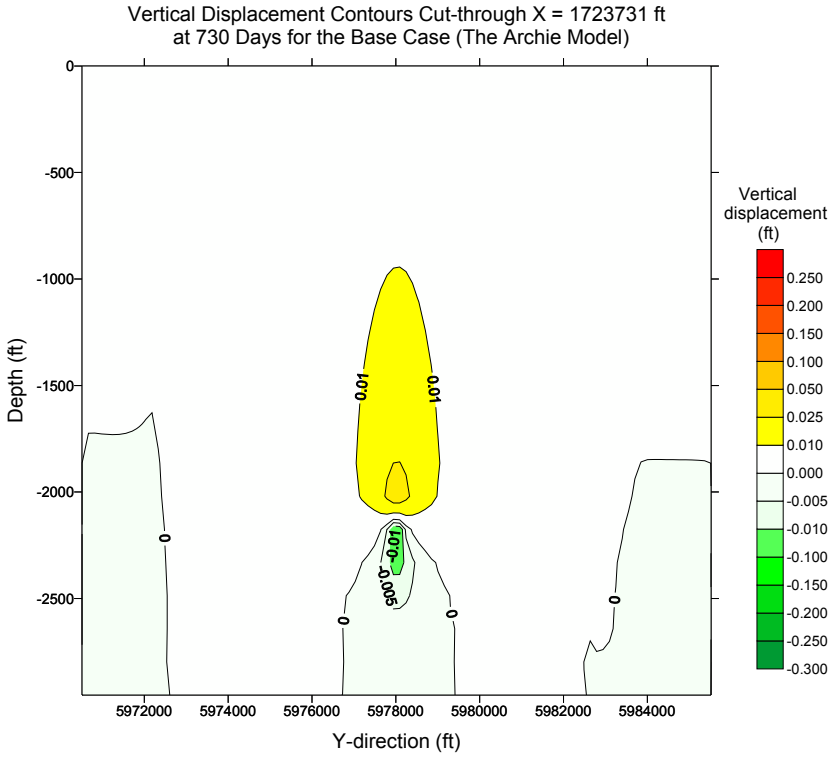

(b) The Archie model

Figure 2-23: Contour maps showing vertical displacements cut-through X = 1723731 ft at 730 days for the base case in the PBU L-pad area (AIM model vs. Archie model).

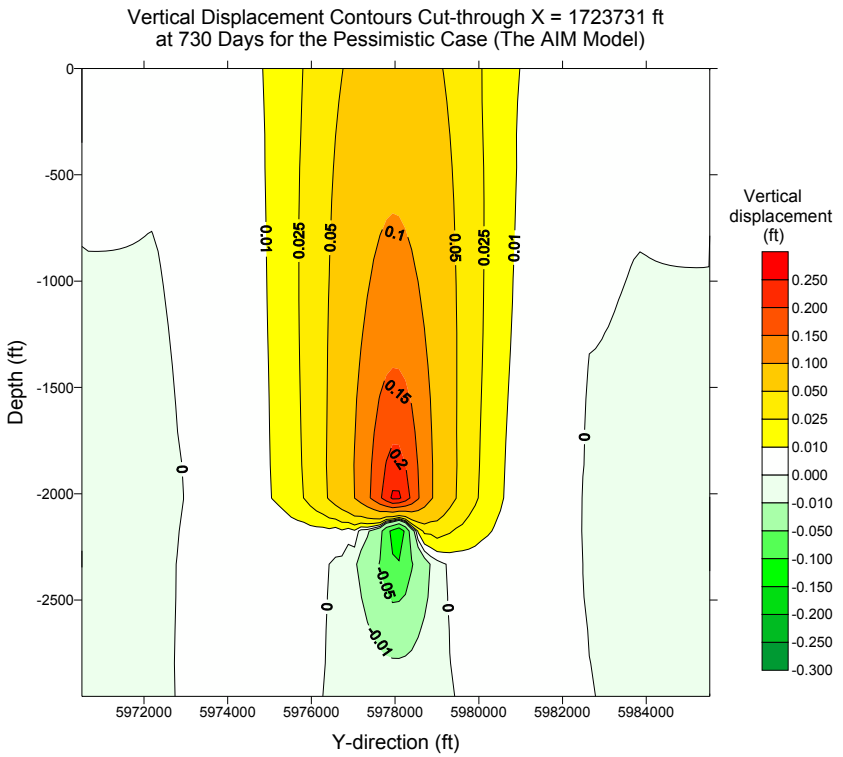

(a) The AIM model

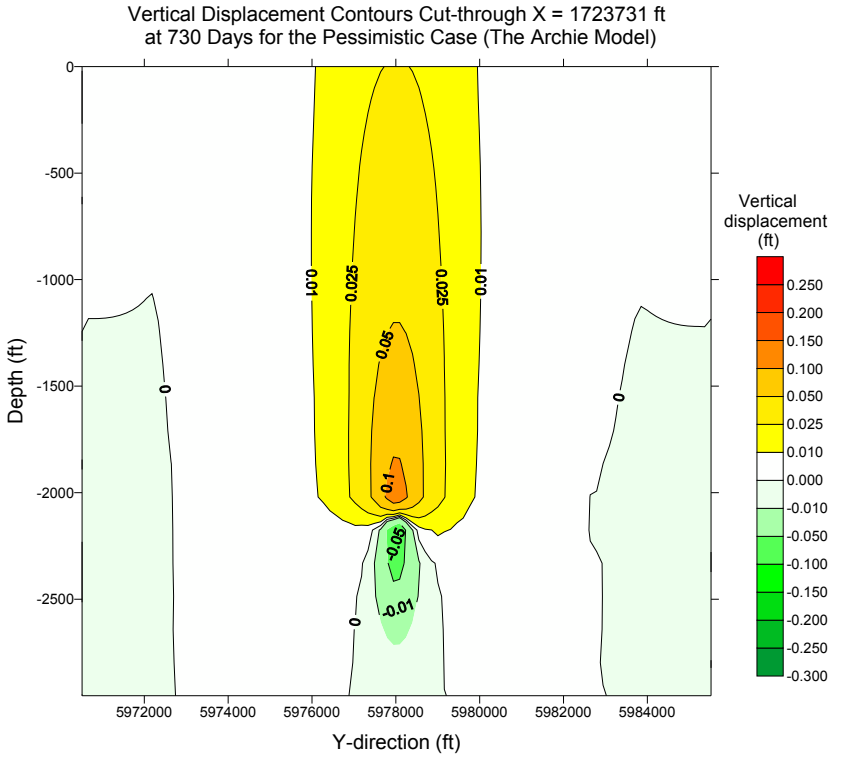

(b) The Archie model

Figure 2-24 Vertical displacements cut-through X = 1723731 ft at 730 days for the pessimistic case in the PBU L-pad area (AIM model vs. Archie model).

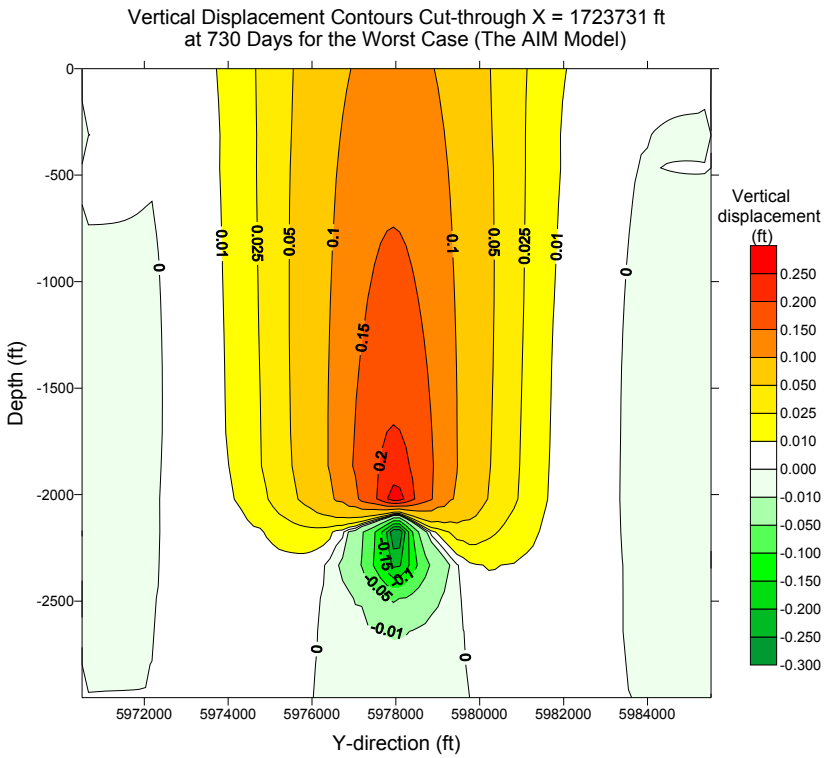

(a) The AIM model

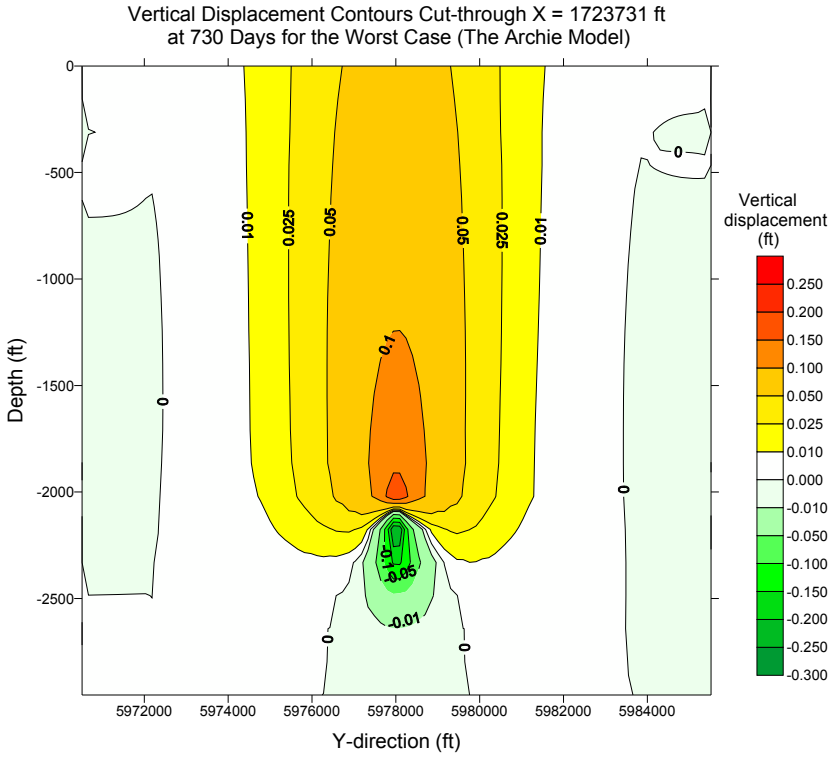

(b) The Archie model

Figure 2-25. Vertical displacements cut-through X = 1723731 ft at 730 days for the worst case in the PBU L-pad area (AIM model vs. Archie model).

IV. CONCLUSIONS

Results of this surface subsidence study for the PBU L-Pad area on the North Slope of Alaska are provisional because the mechanical properties of overburden rock and reservoir rock used in the model contain uncertainties and are not directly measured from laboratory and/or field measurements, and the geological description of the overburden is estimated from well log data. The surface subsidence prediction using the subsidence model for the methane hydrate reservoir can be further improved as rock mechanics data from laboratory tests and field measurements and a more rigorous constitutive model for methane hydrate reservoir rock become available in the future.

1. A full-field, 3D subsidence model is developed for the methane hydrate reservoir at the PBU L-pad area. The developed model is coupled with the TOUGH+Hydrate reservoir model through geological and geometric descriptions of the reservoir section and uses input data based upon TOUGH+Hydrate simulation results. The developed subsidence model is a useful tool for calculating the surface subsidence for a given methane hydrate production case by pressure depletion (depressirization) in the PBU L-pad area.

2. Predicted peak surface subsidence in the PBU L-pad area increases with time as methane hydrate production by pressure depletion proceeds. Depending upon cases investigated, peak surface subsidence ranges from 0.006 to 0.118 feet at producing time 730 days for the 2-year gas production case investigated. These cases include the base case, the pessimistic case, and the worst case. The maximum subsidence value 0.118 feet predicted from the unlikely worst case suggests that the impact of methane hydrate production by pressure depletion on surface subsidence in the PBU L-pad area is not significant.

3. The AIM model predicts higher subsidence values than the Archie model for all cases studied. Thus, it is important to accurately estimate initial hydrate saturation for reducing the uncertainty in subsidence prediction.

4. Contour maps of surface subsidence have been generated from the simulation results for the base case, the pessimistic case, and the worst case studied at producing time 730 days by pressure depletion of the hydrate reservoir in the PBU L-pad area.

5. Contour maps of vertical displacements on the cross-section in the East-West cut and in the North-South cut through the center of the modeled domain have been generated from the simulation results for the base case, the pessimistic case, and the worst case studied.

V. REFERENCES

1. Chin, L.Y. and Boade, R.R. 1990. *Full-Field, Three-Dimensional Computer Modeling of Reservoir Compaction and Subsidence at Ekofisk*. Copenhagen: Third North Sea Chalk Symposium.

2. Chin, L.Y. and Nagel, N.B. 2004. *Modeling of Subsidence and Reservoir Compaction Under Waterflood Operations.* International Journal of Geomechanics, v. 4 , no. 1, p. 28-34.
3. Terzaghi, K. 1943. *Theoretical Soil Mechanics.* New York: Wiley.
4. Hughes, J.R. Thomas. 1987. *The Finite Element Method.* Englewood Cliffs, New Jersey: Prentice-Hall.

National Energy Technology Laboratory

626 Cochrans Mill Road
P.O. Box 10940
Pittsburgh, PA 15236-0940

3610 Collins Ferry Road
P.O. Box 880
Morgantown, WV 26507-0880

13131 Dairy Ashford, Suite 225
Sugarland, TX 77478

1450 Queen Avenue SW
Albany, OR 97321-2198

2175 University Ave. South
Suite 201
Fairbanks, AK 99709

Visit the NETL website at:
www.netl.doe.gov

Customer Service:
1-800-553-7681